

Discerning Changes in High-Frequency Climate Variability using Geochemical Populations of Individual Foraminifera

Ryan H. Glaubke^{1,2}, Kaustubh Thirumalai³, Matthew W. Schmidt¹, and Jennifer E. Hertzberg¹

¹Department of Ocean, Earth, and Atmospheric Sciences, Old Dominion University, Norfolk, VA, USA

²Department of Marine and Coastal Sciences, Rutgers University, New Brunswick, NJ, USA

³Department of Geosciences, University of Arizona, Tucson, AZ, USA

Corresponding author: R. H. Glaubke (rglaubke@marine.rutgers.edu)

Key Points:

- QUANTIFA is an open-source algorithm that models IFA-related uncertainties and analyzes IFA data.
- By simulating past changes in climate variability, users can estimate IFA detection sensitivity throughout the tropical ocean.
- QUANTIFA also provides a robust statistical framework that streamlines and standardizes IFA data analysis.

This article has been accepted for publication and undergone full peer review but has not been through the copyediting, typesetting, pagination and proofreading process, which may lead to differences between this version and the Version of Record. Please cite this article as doi: 10.1029/2020PA004065.

Abstract

Individual Foraminiferal Analysis (IFA) has proven to be a useful tool in reconstructing the amplitude of high-frequency climate signals such as the annual cycle and the El Niño – Southern Oscillation (ENSO). However, using IFA to evaluate past changes in climate variability is complicated by many factors including geographic location, foraminiferal ecology, methods of sample processing, and the influence of multiple, superimposed high-frequency climate signals. Robust statistical tools and rigorous uncertainty analysis are therefore required to ensure the reliability of IFA-based interpretations of paleoclimate change. Here, we present a new proxy system model—called the Quantile Analysis of Temperature using Individual Foraminiferal Analyses (QUANTIFA)—that combines methods for assessing IFA detection sensitivity with analytical tools for processing and interpreting IFA data to standardize and streamline reconstructions employing IFA-Mg/Ca measurements. Model exercises with simulated and real IFA data demonstrate that the dominant signal retained by IFA populations is largely determined by the annual-to-interannual ratio of climate variability at a given location and depth and can be impacted by seasonal biases in foraminiferal productivity. In addition, our exercises reveal that extreme quantiles can be reliable indicators of past changes in climate variability, are often more sensitive to climate change than quantiles within the distributional interior, and can be used to distinguish changes in interannual phenomena like ENSO from seasonality. Altogether, QUANTIFA provides a useful tool for modeling IFA uncertainties and processing IFA data that can be leveraged to establish a history of past climate variability.

Plain Language Summary

The chemistry of fossil shells formed by marine protists called "foraminifera" has been a valuable tool for reconstructing long-term trends in past climate change. However, establishing a history of important climate phenomena that occur on timescales more relevant to humans, like the strength of the seasonal cycle or the intensity of El Niño events, is much more difficult to achieve. Recently, researchers have begun to address these questions by analyzing individual foraminiferal shells through a technique called Individual Foraminiferal Analysis (IFA). Populations of these individually analyzed shells give us a snapshot of how variable Earth's climate was in the past. However, comparing estimates of climate variability between two distinct time periods, like between our present warm period and the last Ice Age, requires stringent statistics and rigorous estimates of uncertainty. In this paper, we introduce an algorithm designed to handle these challenges by mimicking laboratory sampling procedures on a virtual sediment sample modeled after real oceanographic data. The algorithm also incorporates a set of statistical tools that aid the user in deciphering the patterns exhibited by their data. We then demonstrate how it can be a helpful new tool for the research community to quickly process and interpret IFA data.

1. Introduction

The geochemical composition of foraminiferal calcite has served as the backbone of paleoceanographic reconstructions for decades and has been a critical tool in developing our understanding of the ocean's role in past climate change (Kucera, 2007). Conventionally, long-term records from marine sediment cores are generated by pooling and analyzing multiple monospecific foraminiferal shells, generating a single datum for each stratigraphic layer that represents an average of oceanic conditions at that time. However, in recent years, advances in

analytical precision coupled with growing interest in reconstructing past changes in high-frequency (i.e. sub-millennial) climate signals—such as the annual cycle and the El Niño – Southern Oscillation (ENSO)—has led to the development of a novel single-shell analytical technique known as Individual Foraminiferal Analysis, or IFA (Koutavas et al., 2006; Leduc et al., 2009b; Wit et al., 2010; Ganssen et al., 2011; Khider et al., 2011; Scroxton et al., 2011; Koutavas and Joanides, 2012; Sadekov et al., 2013; Rustic et al., 2015; Vetter et al., 2017; White et al., 2018; Schmitt et al., 2019; Thirumalai et al., 2019; White and Ravelo, 2020; Rustic et al., 2020). By virtue of the two- to four-week life span of most planktic foraminifera (Spero, 1998), the geochemical signature of a single shell represents a quasi-monthly "snapshot" of the ambient ocean conditions in which the shell precipitated. Thus, differences in shell chemistry among individual foraminifera from the same stratigraphic layer nominally represent a composite sample of hydrographic variability over the timescale represented by the core interval (Thirumalai et al., 2013).

In regions of the global ocean where hydrographic variability is strongly influenced by a particular climate oscillation, relative differences between IFA populations can be used to resolve changes in the amplitude of that oscillation through time. However, interpreting IFA population distributions as a reflection of past climate variability is not straightforward and can be complicated by (1) the influence of multiple, superimposed high-frequency climate signals, and (2) uncertainties associated with a number of environmental, biological, and sample processing factors (Thirumalai et al., 2013; Wit et al., 2010; Groeneveld et al., 2019). Thus, the quality and reliability of IFA-based reconstructions rests heavily on the strength of the statistical methods applied to disentangle competing climatic influences and constrain sources of uncertainty.

Recent efforts to successfully disentangle the signal-of-interest from the "noise" of ambient background climate have led to improvements in how IFA data are processed and interpreted. In earlier studies, differences between IFA distributions were characterized through direct comparison of parametric measures of scale such as standard deviation and variance (Koutavas et al., 2006; Koutavas and Joanides, 2012; Leduc et al., 2009b; Sadekov et al., 2013). The problem with the approach, however, is that it relies on a priori assumptions regarding the normality of the underlying climate signal (Lanzante, 1996). Aside from concerns regarding the influence of outlying values (Lanzante, 1996) or the non-gaussian behavior of climate oscillations such as ENSO (Khider et al., 2011), these metrics only provide a simple measure of population spread that, by design, ignores variability in the overall shape and structure of IFA distributions. Such differences could hold climatically meaningful information that allows researchers to distinguish the relative influence of overlapping high-frequency climate signals with inherently different time scales. More recent IFA studies have been successful in characterizing variability in IFA distributional shape by employing quantile-quantile (Q-Q) analysis—a common yet powerful and statistically robust tool for comparing distribution data (Ford et al., 2015; White et al., 2018; Thirumalai et al., 2019; White and Ravelo, 2020; Rustic et al., 2020). By plotting the evenly-spaced quantiles of one data distribution against another, Q-Q plots capture differences in location, scale, and skew in one convenient plot, without the need for any underlying assumptions regarding the data (Lodder and Heiftje, 1988). Moreover, Q-Q analysis is capable of detecting differences between particular regions of a data distribution such as within the interior or out in the tails—whereas traditional metrics characterize data

distributions holistically. Recent IFA work suggests this latter feature of Q-Q analysis is valuable for parsing changes in annual vs. interannual climate phenomena (Ford et al., 2015; White et al., 2018; Thirumalai et al., 2019; White and Ravelo, 2020; Rustic et al., 2020). For example, in the equatorial Pacific, ENSO events are typically characterized by large sea surface temperature (SST) anomalies that exceed the total seasonal temperature range (Wang and Fielder, 2006). As a result, changes in ENSO amplitude could ostensibly be inferred from IFA paleotemperature distributions as differences in the extent of the tails, with changes in the annual cycle presumably confined to the middle of the distribution (Ford et al., 2015; White et al., 2018; White and Ravelo, 2020; Rustic et al., 2020).

At the same time, however, a combination of environmental, biological, and sample processing factors can also have a significant impact on the shape and structure of IFA distributions. complicating interpretations of past climate variability. For example, the relative influence of annual and interannual climate phenomena on a region's hydrographic variability can vary significantly, both laterally and with depth (Thirumalai et al., 2013). As a result, the location of a sediment core and the mean calcification depth of the foraminiferal species used for the reconstruction exerts a first order control on the ability of IFA distributions to detect certain climate signals. Further complications arise when considering changes in foraminiferal ecology (Groeneveld et al., 2019) and post-depositional effects such as bioturbation (Dolman et al., 2018). In addition, the physical recovery of IFA distributions is associated with its own sources of uncertainty, including: (1) sampling error, related to IFA population size; (2) analytical error, determined by instrument precision; and (3) calibration error, introduced when translating raw geochemical values to inferred environmental parameters (Thirumalai et al., 2013). The impact of sampling error can be especially influential on the tails of IFA distributions, where the presence/absence of outlying values have led some to questions their reliability as indicators of past climate variability. Thus, one of the outstanding challenges in IFA Q-Q analyses rests in developing methods that weigh the impact of climate signals vs. other external influences on quantile behavior.

One approach to constraining these uncertainties is to utilize proxy system models that capture the translation of high-frequency climate signals into fossil foraminiferal populations and replicate their recovery by simulating the selection and analysis of individual foraminifera (Dolman et al., 2018; Evans et al., 2013). An early study to adopt this approach introduced the Individual Foraminiferal Approach Uncertainty Analysis (INFAUNAL) algorithm (Thirumalai et al., 2013), which has been used to estimate IFA detection sensitivity at a particular location by modeling changes in IFA- δ^{18} O population spread in response to prescribed changes in highfrequency climate variability (Thirumalai et al., 2013). However, INFAUNAL primarily relies on standard metrics of population spread such as standard deviation and range. At present, a similar tool that constrains variability in the shape and structure of IFA distributions is not yet available. Moreover, there is currently no proxy system model available that explores the uncertainties inherent to IFA reconstructions derived from magnesium-to-calcium (Mg/Ca) ratios of foraminiferal calcite, an arguably more direct proxy for ocean temperature variability (Ford et al., 2015; White et al., 2018; White and Ravelo, 2020; Rustic et al., 2020). Although recent IFA-Mg/Ca studies have independently developed and incorporated their own form of uncertainty analysis, methods vary between studies (see, e.g., uncertainty analyses conducted by Ford et al., 2015 vs. Thirumalai et al., 2019). A centralized computational tool for IFA-related uncertainty

analysis and data processing could provide a common statistical framework that standardizes IFA data analysis and streamlines future reconstructions of seasonality, ENSO, and other high-frequency climate signals (Greene and Thirumalai, 2019).

To that end, we developed a user-friendly proxy system model, called the Quantile Analysis of Temperature using Individual Foraminiferal Analyses (QUANTIFA), that combines rigorous uncertainty analysis with robust analytical tools to provide a standardized statistical framework for IFA data analysis. Using INFAUNAL as a basis (Thirumalai et al., 2013), we combine pseudoproxy forward-modeling techniques with a bootstrap resampling scheme to constrain variability in IFA distributional shape in response to prescribed changes in climate variability. However, OUANTIFA goes one step further by combining INFAUNAL's core function of modeling IFA detection sensitivity with a data processing element that both facilitates O-O analyses of two inputted IFA populations and performs additional analyses that aid the user in deciphering the significance of their results. These analyses include false positive tests that estimate the frequency of type I errors, as well as a data-model consistency analysis that compares the user's results against modeled results from hypothetical scenarios of altered highfrequency climate variability. This combination of conventional Q-Q analyses with estimates of uncertainty, detection sensitivity, false positivity, and data-model consistency builds a unique interpretative framework that can more thoroughly inform IFA-based interpretations of past climate variability. In this work, we first detail the statistical and mathematical basis our new algorithm. We then utilize QUANTIFA to explore the influence of IFA sample size on the feasibility of using extreme quantiles in the tails to diagnose changes in high-frequency climate variability. Finally, we apply our algorithm to three previously published IFA datasets from throughout the tropical Pacific Ocean. Our model exercises demonstrate QUANTIFA's potential as a useful exploratory and data analysis tool that can help bolster the efficiency and accuracy of future IFA-based reconstructions.

2. Model Description

QUANTIFA is an open-source proxy system model available for MATLABTM designed to (1) test the ability of the IFA technique to resolve changes in high-frequency climate variability, primarily focusing on seasonality and ENSO, and (2) establish a statistical and interpretive framework for analyzing IFA data (Figure 1). Accordingly, QUANTIFA is flexible in its use. Without the input of IFA data, the algorithm can be used to model the sensitivity of paleotemperature distributions to changes in the amplitude of annual and interannual climate variability. This is achieved by simulating the IFA sampling procedure (along with its associated uncertainties) on modeled pseudoproxy time series representing both modern climate conditions and hypothetical scenarios of altered climate variability. Alternatively, QUANTIFA can be used as an analytical tool for comparing down-core IFA populations or for comparing core-top populations with modern reanalysis data (this latter exercise is not performed here, although the algorithm includes documentation for such a procedure). QUANTIFA identifies significant differences between the two distributions by coupling Q-Q analysis with an iterative bootstrapping subroutine that constructs uncertainty envelopes incorporating analytical, calibration, and sampling errors. In addition, QUANTIFA provides an interpretive framework to aid the user in deciphering the pattern exhibited by their data. This framework includes a series of false positive tests to provide a measure of reliability in the observed results, as well as data-

model consistency maps that compare the configuration of the user's quantiles in Q-Q space against simulated quantiles from each modeled climate scenario.

2.1 Pseudoproxy Time Series

Both of QUANTIFA's core applications—modeling IFA detection sensitivity and facilitating IFA population comparisons—rely on creating a collection of synthetic Mg/Ca time series that simulate paleodata entrained within an idealized virtual sediment sample (Figure 1). These time series are constructed using subsets of the Ocean Reanalysis System 5 (ORA-S5) data assimilation containing a three-dimensional gridded field of potential temperature data (Zuo et al., 2019). In our model exercises below, we utilize a subset spanning the tropical Pacific Ocean $(30^{\circ}N - 30^{\circ}S, 120^{\circ}E - 70^{\circ}W; 0 - 5902 \text{ m})$, although we note that subsets from the tropical Atlantic and Indian Oceans are also available for use with OUANTIFA (see section 4). The ORA-S5 data structures have a 1° x 1° horizontal resolution and 75 depth levels, with the highest vertical resolution in the upper 200 m where most planktic foraminifera live. Each grid box contains a 61-year time series of monthly mean potential temperature data extending from Jan 1958 – Dec 2018. Using coordinates and depth information prescribed by the user (**Table 1**), QUANTIFA extracts the temperature time series from the nearest ORA-S5 grid box and converts the values into Mg/Ca ratios (in mmol/mol) using a calibration equation specified by the user. Users can either select from a set of pre-programmed calibration equations (see Table S1 for a complete list) or incorporate their own. Additionally, QUANTIFA can be coupled to Bayesian, multivariate Mg/Ca calibration models (such as those by Khider et al., 2015, Tierney et al., 2019, and Holland et al., 2020) to account for factors other than temperature that influence foraminiferal Mg/Ca. It should be noted, however, that (to our knowledge) all existing foraminiferal Mg/Ca-T calibrations have been developed using multi-specimen samples. Therefore, absolute temperatures calculated from IFA data using these equations may produce different results than if a calibration developed from individual foraminifera was used.

The resulting forward-modeled Mg/Ca time series is used to generate a number of pseudoproxy time series covering a broad range of potential paleoclimate scenarios. First, the algorithm models paleodata reflective of modern climate variability (hereafter referred to as the "modeled modern time series"). Following procedures adopted from INFAUNAL (Thirumalai et al., 2013), QUANTIFA calculates monthly averaged Mg/Ca ratios for all neutral (i.e., non-ENSO) years to establish a mean seasonal climatology at the location. Monthly mean Mg/Ca ratios are also calculated for all El Niño and La Niña years (as identified by the Oceanic Niño Index) and subtracted from the base climatology to establish monthly mean anomalies associated with ENSO. To extend the modeled modern time series and match it to the theorized length of time represented by the sediment sample, QUANTIFA repeatedly splices the climatological seasonal cycle for a number of years specified by the user (**Table 1**). El Niño and La Niña events are inserted into the time series by adding the ENSO anomalies atop this annual cycle. Finally, to ensure that the modeled paleodata are similar to the instrumental record both visibly and in frequency space, red and white noise is added to the time series.

QUANTIFA then generates a collection of pseudoproxy time series representing hypothetical scenarios of altered climate variability by gradually modifying the amplitude of the seasonal cycle and ENSO events within the modeled modern time series. We opted not to adjust the number of ENSO events in our altered climate time series given prior evidence that ENSO

frequency has little-to-no control over the IFA signal (Thirumalai et al., 2013). Seasonality is altered by amplifying/damping the magnitude of the quasi-sinusoidal seasonal climatology calculated from the forward-modeled Mg/Ca data. To manipulate ENSO amplitude, the Mg/Ca anomalies associated with ENSO events are modified so that the events can grow in phase and peak with the annual cycle. Both seasonality and ENSO amplitude are adjusted in 10% increments, ranging from a complete damping of the signal (-100%) to a doubling of the signal (+100%), generating 440 altered climate scenarios with different permutations of seasonality and ENSO change (Thirumalai et al., 2013).

We acknowledge that this method of statistically modeling altered states of climate variability relies on the assumption that the structure of month-to-month patterns in seasonality and interannual anomalies at a given location does not change with time. Changes in the relative strength or the spatial footprint of these phenomena, such as what has been suggested for the ENSO during the last glacial period (Liu et al., 2020), could represent a potential limitation of our forward modeling scheme.

2.2 Modeling IFA Detection Sensitivity

QUANTIFA assesses the ability of IFA populations to resolve changes in annual and interannual climate variability by simulating the IFA sampling procedure on the modeled time series and subjecting the resulting pseudo-IFA populations to Q-Q analysis (**Figure 1**). First, QUANTIFA constrains the uncertainties associated with the IFA approach by employing a smoothed bootstrap resampling scheme (Efron, 1979) designed to simulate the random selection of individual foraminifera from a sediment sample, as well as the errors associated with their analysis and translation to paleotemperature values. The algorithm repeatedly selects monthly mean Mg/Ca ratios from each modeled time series to produce pseudo-IFA populations for a set number of realizations. Each population is then converted into a paleotemperature distribution following the calibration equation prescribed by the user at the beginning of the model run. At each step within this "picking loop", uncertainties associated with analytical precision and calibration error are incorporated as Gaussian distributions (1 σ defined by the user; **Table 1**), creating a range where picked Mg/Ca ratios and translated paleotemperature values are permitted to vary.

QUANTIFA then performs a series of Q-Q analyses that compare all modeled paleotemperature distributions from the altered climate scenarios against those generated from the modeled modern time series, an exercise analogous to performing down-core IFA population comparisons (**Figure 1**). In doing so, QUANTIFA produces multiple Q-Q realizations that approximate the uncertainty related to subsampling a larger population. To emphasize differences between the two populations apart from changes in mean temperature, each paleotemperature distribution is centered before quantiles are computed. The algorithm sorts the modeled quantiles into bins according to their proximity along the x-axis to the mean quantiles of the modeled modern time series (calculated by averaging across model realizations). Within each bin, the algorithm computes: (1) the mean of the binned quantiles, (2) the standard deviation, and (3) the mean distance each quantile falls from the 1:1 line, hereafter referred to as "residuals". Residuals are used to characterize the overall shape of the quantiles in Q-Q space. For example, if two distributions are closely identical, the quantiles within each bin will cluster tightly around the 1:1 line, and the corresponding mean residual values would be near zero. The larger the difference

between the two distributions, the further the cloud of Q-Q realizations will deviate from the 1:1 line, resulting in greater mean residuals. This exercise is repeated for all altered climate scenarios, creating a set of mean quantiles and residuals that describe a characteristic shape in Q-Q space corresponding to a particular configuration of ENSO and seasonality change when compared to modern climate conditions.

QUANTIFA uses these idealized Q-Q patterns to assess the response of paleotemperature distributions to changes in high-frequency climate variability. To better characterize the dominant climatic influences within different parts of the paleotemperature distribution, mean residual values are sorted into three distinct regions: the interior of the distribution (the middle 68%) and the warm and cold tails (the upper and lower 16%, respectively). The algorithm computes the proportion of the quantiles within each group that fall within $\pm 1\sigma$ from the 1:1 line, a range we define as exhibiting close conformity with the "modern" distribution. Populations from the altered climate scenarios that conform closely with the shape of the "modern" distribution would return high conformity values (%) for each region and would, in theory, be difficult to detect in real IFA populations. Scenarios with poor conformity indicate large differences between the "altered" and "modern" distributions, suggesting a high probability of detection. The calculated percent of conformity for each Q-Q comparison is displayed on a contour plot, where the structure of the contours can be used as a visual diagnostic for relative signal strength (ENSO vs. seasonality) and IFA detection sensitivity. Contours with a fully vertical orientation, for example, indicate a sensitivity to changes in ENSO amplitude, while horizontal contours indicate a greater sensitivity to seasonality. Diagonal contours, by extension, would suggest some combination of both. Likewise, the gradient of the plotted contours can be used to infer detection sensitivity. Contours plotted close to one another would suggest heightened sensitivity to a particular climate signal, and contours plotted farther apart would suggest the opposite.

2.3 Processing IFA Data and Building an Interpretive Framework

In addition to modeling IFA detection sensitivity, QUANTIFA can be used as an analytical tool to compare real IFA populations against one another or to compare an IFA population with modern reanalysis data (Figure 1). Inputted IFA-Mg/Ca data are first converted into paleotemperature values with user-selected calibrations, centered, and then subdivided into quantiles. To identify potential differences between the two populations (or between an IFA population and the reanalysis data), QUANTIFA constructs uncertainty envelopes by repeatedly resampling the modeled modern time series using the same "picking loop" and binning strategy detailed in section 2.2. This exercise is performed twice: once to derive error in the X direction and again for error in the Y direction. The only difference between the two operations is the size of the resulting pseudo-IFA populations, which is determined by the size of the IFA dataset assigned to that axis. QUANTIFA produces a Q-Q plot of the user's data that includes an inset with a smoothed, gaussian kernel density estimate of the inputted IFA populations, emphasizing differences between the shapes of the two distributions reflected in the Q-Q plot. We stress that our choice in kernel function has no bearing on the results of the Q-Q analyses, given that the quantiles are computed from the raw data. The Q-Q plots also include uncertainty bounds at a user-specified degree of confidence: 85%, 90%, 95%, or 99% (Table 1). Whenever a quantile deviates from the 1:1 line beyond this region of uncertainty, it is considered significantly different at that corresponding level of confidence.

Built within the data processing element of QUANTIFA are two additional routines that together constitute an interpretative framework intended to help make sense of any observed differences between two IFA distributions. The first plank of this framework involves conducting false positive tests at the individual quantile level to quantify how often each may commit a type I error—that is, how often a quantile reports a spuriously significant result when the two IFA distributions are known to come from the same population. This is achieved by repeatedly subsampling the site-specific modeled modern time series (using the same "picking loop" detailed above) to generate two pseudo-IFA populations, comparing them via Q-Q analysis, and tallying how often each quantile significantly deviates from the 1:1 line beyond the specified level of confidence. In essence, these false positive rates are meant to serve as a simple measure of a quantile's "reliability" as an indicator of past climate variability. For example, if a quantile—say, an extreme quantile in the tails of a distribution—reports a high false positive rate, then its significance in the user's data should not be taken as a sign of changes in climate variability. Although potential drivers behind high false positive rates—a region's particular climatology, sampling exceedances when partitioning a small IFA population into too many quantiles, etc.—should ultimately be left to the user to investigate, QUANTIFA's false positive tests provide a simple yet powerful measure of assessing a quantile's climatic significance.

The second plank of QUANTIFA's interpretive framework involves constructing data-model consistency maps, where the position of the user's significant quantiles in Q-Q space is compared against the position of those same quantiles from each hypothetical climate scenario (**Figure 1**). The purpose of this exercise is to highlight the set of altered climate scenarios that most closely conform to the user's data, providing a foundation from which to infer past changes in climate variability. To this end, QUANTIFA first identifies and calculates the residuals of user quantiles which significantly deviate from the 1:1 line. Next, the algorithm assesses data-model fit by calculating a parameter called the residual difference (ΔR), which we define as the difference between the residual of the user's quantile and the mean residual values for that quantile from each altered vs. modern Q-Q comparison:

$$\Delta R = \left| R_{Q_{user}} - R_{Q_{model}} \right| \tag{1}$$

where $R_{Q_{user}}$ refers to the residual of quantile Q of the user's data, and $R_{Q_{model}}$ represents a 21 x 21 matrix of mean residual values for quantile Q from each hypothetical climate scenario. Applying equation (1) to each significant quantile generates a matrix of ΔR values which reflect the quantile's "goodness-of-fit" for each hypothetical scenario, where the lower the ΔR value (i.e., the smaller the difference between the user's residuals and the modeled residuals), the better the fit. Climate scenarios where the ΔR value is less than the 1σ error for that quantile are identified by QUANTIFA as a scenario that exhibits good data-model consistency. The algorithm then collates the ΔR matrices for each significant quantile and calculates the proportion of those quantiles that exhibit good data-model fit for each climate scenario. These proportions are presented as heat maps, where regions of high percentages indicate the set of hypothetical climate scenarios that are most consistent with the user's data. We emphasize that, given the inherent uncertainties associated with IFA, data-model consistency results for an individual climate scenario can vary slightly across model runs. Therefore, these maps should be used as *qualitative* diagnostic tools for identifying broad patterns of high-frequency climate

change (e.g., enhanced vs. reduced variability) rather than attributing user results to a specific scenario of altered climate variability. Any quantitative interpretations should be carefully and independently vetted. Nevertheless, these data-model consistency maps are a useful tool for deciphering the signals preserved within IFA populations.

3. Model Application Exercises

To demonstrate the utility of QUANTIFA as an exploratory and data analysis tool, we perform two different exercises. In the first, we explore the influence of IFA sample size on extreme quantile behavior to better understand under what circumstances the tails of IFA distributions can be viewed as reliable indicators of high-frequency climate change, given their sensitivity to outlying values. We perform a series of false positive tests on pseudo-IFA populations of variable sample sizes (n = 25, 50, 75, 100, 125,and 150) derived from forward-modeled SSTs in the Niño 3.4 region. We hold the number of quantiles constant at 50, to see whether over- or under-discretization of the paleotemperature distribution also plays a role in extreme quantile behavior.

In the second exercise, we conduct three case studies where we apply QUANTIFA to previously published IFA datasets collected throughout the tropical Pacific. For each case, we conduct a sensitivity analysis to constrain the relative influence of annual and interannual climate variability over the IFA signal at the core location (see **Text S1** for details on model input). We then run the IFA data through QUANTIFA to identify any significant differences between the two populations and attribute these differences to changes in ENSO or seasonal cycle amplitude (or some combination of both). We stress that the purpose of this latter exercise is not to investigate the underlying mechanisms that could produce any observed changes in high-frequency climate variability. Instead, our purpose is to illustrate how the individual output products generated by QUANTIFA can by brought together to more thoroughly inform interpretations of past climate variability.

3.1 Exploring the Influence of Sample Size on Tail Sensitivity in the Niño 3.4 Region Repeated subsampling and Q-Q analysis of pseudo-IFA populations from the Niño 3.4 region consistently report low levels of false positive results at the 90% confidence level for all extreme quantiles regardless of sample size, with mean rates remaining below 6% (**Figure 2**). Interestingly, with regards to the warm tail, our estimates closely match those reported by Rustic et al. (2020), despite their use of an algorithm that employs a different analytical approach for constraining uncertainty. However, stress testing our results by running the model exercise 100 times (each with 5,000 Q-Q realizations) reveals a considerable degree of variability, with the largest differences often observed *between* quantiles rather than among different sample sizes *within* a single quantile. According to our results, the relationship between false positive rate and IFA sample size is inconsistent. For example, smaller IFA sample sizes do not always report higher false positive rates, while larger IFA sample sizes do not necessarily reduce the risk of a false positive result. As such, it appears IFA sample size does not have an impact on an individual quantile's false positive rate, even in cases where the number of quantiles exceeds the total number of individual foraminifera that comprise the IFA distribution.

Instead, inter-quantile differences are more readily apparent, with variability in false positive rates tending to be greatest for tail quantiles than for those in the distributional interior (Figure S1). The exact pattern of false positive rates between the cold and warm tails is not symmetrical, however, which can likely be attributed to the region's particular climatological response (asymmetries in warm and cold anomalies of the underlying time series force differences in the response of warm and cold tails). As such, the quantiles with the highest mean false positive rates are not always the most extreme quantiles, as might be expected. Regardless, tail quantiles remain quite variable, with rates reaching >20% in some cases (although this is very rare: ~0.13% of 300,000 computed rates). In most cases (94%), false positive rates remain below 10% for all quantiles across all sample sizes, which approximates the presumed probability of type I error based on our 90% confidence envelopes. Therefore, it seems reasonable to conclude that tail quantiles can be viewed as generally reliable indicators of past climate variability. However, it should be emphasized that this conclusion is highly dependent on the dynamics of the underlying reanalysis time series, which varies with location and depth. Our exercise thus highlights the importance of integrating estimates of false positive rates into QUANTIFA's interpretive framework, so similar analyses can be conducted for a user's region of interest.

3.2 Case Studies from the Tropical Pacific

3.2.1 The Western Tropical Pacific

For our first case study, we use Holocene and Last Glacial Maximum (LGM) populations of the surface-dwelling species *Globigerinoides ruber* (white variety; *sensu stricto* and *sensu lato* morphotypes) from core MD06-3018 (23°00'S, 166°09'E; 2470 m) off the coast of New Caledonia (**Figure 3**; Schmitt et al., 2019).

Our sensitivity analysis at the core site reveals that the IFA signal preserved by G. ruber populations off the New Caledonian coast is almost exclusively controlled by changes in the strength of the annual cycle. At the core location, peak Mg/Ca anomalies associated with El Niño (-0.06 mmol/mol) and La Niña events (0.09 mmol/mol) are marginal compared to the amplitude of the annual cycle (0.38 mmol/mol), resulting in a high ratio of annual-to-interannual variability (Figure 4). The dominance of seasonality over the New Caledonian IFA signal is reflected in the horizontal orientation of the conformity contours generated by QUANTIFA (Figure 5). According to our results, changing ENSO amplitude (moving to the left and right of the yellow stars in Figure 5) has little to no influence over the shape of the modeled paleotemperature distributions. For example, in a scenario where ENSO is doubled (+100%) and seasonality is held constant, all quantiles from the "altered" distribution exhibit 100% conformity with the "modern" distribution (i.e., no quantiles deviate from the 1:1 line beyond 1σ). The results are similar if ENSO is completely damped (-100%), suggesting that even in the most extreme cases, paleotemperature distributions recorded by G. ruber populations from MD06-3018 are largely insensitive to changes in ENSO amplitude. These results remain unchanged even if we apply a seasonal weighting to QUANTIFA's picking algorithm to account for a mild late summer bias in G. ruber flux to the sediments (Jonkers and Kučera, 2015) (Figure S2). Instead, our modeled paleotemperature distributions from the west Pacific show an acute response to changes in the strength of the annual cycle (moving above and below the yellow stars in Figure 5). Yet, based on the more diffuse contour gradient exhibited by quantiles in the interior (Figure 5b), our results suggest that extreme quantiles in the tails are more sensitive to changes in seasonality than those closer to the median. For example, in a scenario where seasonality is increased by

50% while holding ENSO amplitude constant, quantiles out in the tails of the "altered" distribution exhibit no conformity with the "modern" distribution. Under the same scenario, however, as much as 75% of quantiles in the interior are statistically indistinguishable from modeled modern variability. Despite this asymmetry in detection sensitivity, the annual cycle remains the dominate signal shaping upper-ocean paleotemperature distributions in waters near New Caledonia.

Q-Q analysis of the late Holocene and LGM populations from MD06-3018 reveals three quantiles (out of 30; see supplemental information) that significantly deviate from the 1:1 line with 90% confidence (Figure 6a). Based on our sensitivity analysis above, these quantiles could be indicative of differences in seasonality between the two time slices. False positive rates for all three quantiles are relatively low (mean rates for the 1st, 26th, and the 27th quantiles are 2.99%, 1.13%, and 1.03%, respectively; **Figure S3a**), providing some support for a climate-driven signal. However, with these tools alone, it is difficult to discern the direction of seasonality change. If we compare the position of the three quantiles against the idealized Q-Q patterns for this location, the resulting data-model consistency map reveals broad agreement with scenarios of varying degrees of ENSO amplitude (**Figure 6b**), confirming the relative insensitivity of G. ruber populations from MD06-3018 to changes in interannual climate variability. Regarding the state of the glacial annual cycle, however, the results are ambiguous. QUANTIFA suggests two distinct possibilities: two of the three quantiles are consistent with scenarios of reduced seasonality, whereas a third significant quantile aligns more closely with scenarios of moderately enhanced seasonality (Figure 6b). Therefore, while it could be argued that the MD06-3018 IFA dataset likely represents a reduction in seasonality during the LGM relative to the Holocene, with this dataset and at the present level of confidence, the possibility of an enhanced seasonal cycle cannot be definitively ruled out.

While it is unlikely that these quantiles may have registered as significant by random chance (taking the high end of the standard deviation in our false positive rates, the compounded probability of a type I error is (0.10)(0.04)(0.04) = 0.02%; Figure S3a), it is more likely that at least some of the ambiguity in interpretation can be attributed to the small sample size of the MD06-3018 IFA dataset (n = 30). Smaller sample sizes risk misrepresenting the true shape of the larger population distribution and, as a result, are subject to greater sampling uncertainty (Thirumalai et al., 2013). As such, although a small sample size may not increase the risk of encountering false positives (see section 3.1), it can impact the resolution of the recovered paleotemperature distribution, potentially obscuring tell-tale signs of past climate variability. To illustrate this effect, we run a second sensitivity analysis for the MD06-3018 site but with a larger and more conventional pseudo-IFA population size (n = 70; Thirumalai et al., 2013). Our results show that the estimated 1 σ sampling error for all 30 quantiles (in both X and Y directions) decreases by 36% from an average of 0.28 mmol/mol to 0.18 mmol/mol. Consequently, the conformity contours for this experiment show a contraction in the area of the 100% conformity region and an increase in the conformity contour gradient, both indicators of increased detection sensitivity (Figure S4). Therefore, it is likely that the small IFA dataset from core MD06-3018 underrepresents the true structure of the population distribution, precluding a clear interpretation regarding the state of the annual cycle during the LGM. Supplementing the existing dataset with additional measurements would be required to address this question.

3.2.2 The Central Equatorial Pacific

Next, we compare Holocene and Younger Dryas (YD) populations of the mixed-layer species *Trilobatus sacculifer* from cores MGL1208-14MC and MGL1208-12GC (0°13'S, 155°58'W, 3049 m) recovered from the Line Islands in the central equatorial Pacific (**Figure 3**; White et al., 2018).

Our sensitivity analysis reveals that the IFA signal recorded by T. sacculifer populations in the Line Islands predominantly reflects variability in ENSO amplitude, supporting the inferences made in the original reconstruction (White et al., 2018). At the core site, El Niño and La Niña events are characterized by large Mg/Ca anomalies in the modeled modern time series (0.81 mmol/mol and -0.65 mmol/mol, respectively) that dwarf the amplitude of the mean annual cycle (0.15 mmol/mol), resulting in a small ratio of annual-to-interannual climate variability (**Figure** 7). Consequently, the conformity contours for the central equatorial Pacific exhibit a dramatically different structure than those for the western tropical Pacific (Figure 8). The vertical orientation of the plotted contours signifies that the modeled paleotemperature distributions are insensitive to changes in seasonal cycle amplitude. For example, doubling the strength of seasonality (+100%) or damping it completely (-100%) while holding ENSO amplitude constant results in 100% conformity between the "altered" and "modern" paleotemperature distributions. Thus, large fluctuations in the strength of the annual cycle are not registered by T. sacculifer populations from the Line Islands region. Changing ENSO amplitude, by comparison, alters the modeled paleotemperature distributions in ways that are more readily distinguishable from modern variability. This remains true if we account for a late summer bias in T. sacculifer shell flux observed in a global sediment trap compilation (Jonkers and Kučera, 2015; Figure S5). However, a more diffuse contour gradient and a broad region of 100% conformity exhibited by the quantiles within the middle of the distribution (Figure 8b) suggests that the ENSO signal is most easily detected as changes in the extent of the tails. Moreover, an asymmetry in the contour gradient of the warm and cold tails indicates that extreme quantiles are more sensitive to reductions than enhancements in ENSO amplitude. For example, damping ENSO amplitude by half (-50%) while holding seasonality constant registers as a significant retraction in the tails of the "altered" paleotemperature distribution, resulting in no conformity with the "modern" distribution. In contrast, amplifying ENSO by 50% results in ~40% conformity in the tails. Taken together, our sensitivity analysis provides strong evidence that down-core T. sacculifer populations from the Line Islands preserve a record of ENSO amplitude, with little to no influence from the annual cycle.

Q-Q analysis of the two central Pacific IFA populations reveals enhanced paleotemperature variability during the YD relative to the Holocene (**Figure 9a**). Out of 50 total quantiles (see supplemental information), QUANTIFA identifies 24 that significantly deviate from the 1:1 line with 95% confidence and 11 that deviate with 99% confidence. Notably, the Q-Q results indicate that the greatest differences between the two distributions exist within the interior, where false positive rates are among the lowest (**Figure S3b**) and our sensitivity results suggest a large change in interannual climate variability would be required to drive these quantiles from the 1:1 line. Model fit results reveal broad consistency with scenarios of varied seasonal cycle amplitude that suggests insensitivity towards fluctuations in seasonality, consistent with our analysis above. With regards to ENSO, the greatest concentration of data-model consistency for quantiles at the 95% confidence level align with modeled scenarios of enhanced ENSO amplitude (30±11% of

significant quantiles; **Figure 9b**). Although a few quantiles show some correspondence with scenarios of reduced ENSO variability (18±5% of significant quantiles), the data suggest this can be ruled out almost entirely at a higher (99%) level of confidence (**Figure 9c**). However, we do observe some "patchiness" in our data-model consistency map for quantiles at the 99% confidence level, where scenarios with high data-model correspondence closely adjoin those with lower correspondence. We speculate that this patchiness stems from sources of paleotemperature variability not constrained by our algorithm, which may cause quantiles to diverge from the 1:1 line in a pattern that may contain elements of QUANTIFA's idealized Q-Q patterns from different hypothetical scenarios. In this particular case, this additional source of variability could be driven by decadal-scale climate oscillations, considering that the sampling resolution of cores MGL1208-14MC and 12GC is ~800 years (White et al., 2018). Nevertheless, despite some potential interference from other modes of climate variability, our results collectively advocate for enhanced ENSO amplitude during the YD compared to the Holocene.

Our interpretation is consistent with that of the original study (White et al., 2018), where the authors observe a slight (although statistically insignificant) increase in ENSO amplitude during the YD. Their conclusion was based solely on the behavior of the three warmest quantiles, which they interpret as representing surface ocean temperatures experienced exclusively during El Niño events in the Line Islands region. However, our sensitivity analysis reveals that the behavior of all quantiles responds strongly to changes in ENSO variability and can collectively be leveraged to diagnose past ENSO changes. Our interpretation is also in agreement with transient climate model simulations that indicate amplified ENSO activity during the YD (Liu et al., 2014). We do note, however, that the age of the Holocene population from 14MC (4.03 kyrs) dates to a period of pronounced ENSO reduction, as revealed by paleo-ENSO records recovered from fossil corals (McGregor and Gagan, 2004; Emile-Geay et al., 2016), speleothem deposits (Chen et al., 2016), fossil mollusk shells (Carré et al., 2014), lake sediments (Rodbell et al., 1999; Moy et al., 2002; Conroy et al., 2008), and other marine sediment cores (Rein et al., 2005; Koutavas et al., 2006; Koutavas and Joanides, 2012). Therefore, our interpretation of enhanced YD ENSO amplitude could change if the YD population from MGL1208-12GC was compared against a younger coretop population.

3.2.3 The Eastern Equatorial Pacific

Lastly, we examine Holocene and LGM populations of *T. sacculifer* from ODP Site 849 (0°11'N, 110°31'W, 3851 m) located within the cold tongue extension of the eastern equatorial Pacific (EEP) (**Figure 3**; Ford et al., 2015).

The climatic controls over the IFA signal in the EEP are more complex compared to the western and central Pacific. Variability in mixed-layer temperatures at the core site is driven equally by seasonal fluctuations in upwelling intensity and ENSO phase changes (Wallace et al., 1989; Wang and McPhaden, 2000), resulting in a near even balance between annual and interannual climate variability. Indeed, peak El Niño and La Niña anomalies in the modeled modern time series (0.81 mmol/mol and -0.66 mmol/mol, respectively) are close in magnitude to the amplitude of the annual cycle (0.61 mmol/mol) (**Figure 10**). As a result, paleotemperature distributions derived from *T. sacculifer* populations in the region represent a mixed signal of ENSO and seasonality change which would be difficult to disentangle using conventional metrics such as the standard deviation. The generally diagonal orientation of the conformity

contours indicates that all quantiles respond to some combination of ENSO and seasonality change (**Figure 11**). However, the more horizontally-oriented contours within the interior of the distribution (**Figure 11b**) suggests that quantiles close to the median more readily respond to changes in seasonality than to ENSO. In contrast, quantiles out in the tails, which represent the most extreme temperatures within the EEP, exhibit a relatively vertical orientation (**Figures 11a and 11c**), suggesting that ENSO exerts a greater (although not necessarily consistent) influence over extreme quantile behavior. Notably, the structure of the conformity contours in the warm tail, and to a lesser extent in the cold tail, exhibit a kind of threshold behavior related to the strength of the annual cycle. Under scenarios of reduced seasonality, the contours are mostly vertical in orientation, indicative of a predominant ENSO influence. However, once seasonality is amplified beyond modern day amplitudes (>0%), the structure of the contours changes to a more horizontal orientation, signifying an increased seasonal influence in the extent of the tails. This suggests that although the relative influence of ENSO is greatest in the tails when compared to the distributional interior, this influence can be modified by changes in the strength of the annual cycle.

Collectively, the quantiles from the ODP Site 849 Holocene and LGM populations indicate reduced glacial temperature variability (Figure 12a). QUANTIFA identifies 27 quantiles (out of 50; see supplemental information) that significantly deviate from the 1:1 line: 15 at the 95% confidence level and 12 at the 99% confidence level. Generally, model fit results for quantiles at each level of confidence indicate a region of data-model consistency in the lower half of the heat map, suggestive of reduced glacial seasonality (Figures 12b and 12c). Additionally, we observe a "hot spot" of data-model consistency in the lower left quadrant of the heat map (55±25% of quantiles at 95% confidence and 61±26% of quantiles at 99% confidence), signifying that of the scenarios where seasonality is reduced, those where ENSO is also reduced produce modeled quantiles that best align with the IFA data from ODP Site 849. With respect to ENSO, our results support the conclusions reached by the original reconstruction (Ford et al., 2015), which interpret the data as indicative of a reduced glacial ENSO. However, in attempting to reconcile their results with those from core VM21-30 near the Galápagos (Koutavas and Joanides, 2012), Ford et al. (2015) posit that glacial seasonality could have been enhanced while ENSO was reduced, a prediction consistent with some simulations of past ENSO activity (Chang et al., 1994, 1995; Liu, 2002; Timmerman et al., 2007; Lu et al., 2016). Our reanalysis of the ODP Site 849 dataset instead suggests that both the annual cycle and ENSO amplitude were weakened during the LGM relative to modern conditions, providing support for the idea that ENSO and seasonal cycle amplitude need not have negatively covaried in the past (Emile-Geay et al., 2016).

Notably, these results change slightly if we weigh our picking algorithm to align with maximum *T. sacculifer* productivity in the region. Sediment trap data from the Panama Basin indicates that *T. sacculifer* flux patterns peak during boreal summer (Thunell and Reynolds, 1984). Imposing this seasonal bias in our picking algorithm results in the near complete disappearance of the annual cycle's influence over the EEP IFA signal, leaving ENSO as the dominant force shaping paleotemperature distributions in the region, particularly in the tails (**Figure S6**). Indeed, the new conformity contour structure strongly resembles that from the central Pacific (**Figure 8**). Comparing these new modeled results against observations suggests the IFA data from ODP Site 849 is a more direct indicator of ENSO amplitude change than suggested by the unweighted analysis (**Figure S7**). Although the interpretation implied by the new data-model consistency

maps still suggests that ENSO amplitude was reduced during the LGM relative to the modern day, the near erasure of the annual signal means it cannot address the question of covariance between ENSO and seasonality amplitude changes in the past. This example underscores the importance of considering biases in shell flux when interpreting IFA population variability; in some cases, such as for ODP Site 849, imposing shell flux biases can change the very nature of the scientific questions a user's dataset can address. Moreover, our results reinforce seasonal-weighting exercises conducted using INFAUNAL (Thirumalai et al., 2013), collectively suggesting that seasonal preferences in calcification carry strong implications for reconstructing high-frequency climate signals regardless of choice in either geochemical proxy system (Mg/Ca vs. δ^{18} O) or statistical approach (parametric vs. non-parametric statistics).

4. Summary and Conclusions

In this work, we have detailed a new proxy system model—QUANTIFA—which statistically clarifies the uncertainty and interpretation involved in IFA-Mg/Ca reconstructions. As demonstrated above, using QUANTIFA to model the translation of high-frequency climate signals into fossil foraminiferal populations and to constrain the uncertainties associated with their recovery can be a valuable tool for interpreting IFA data. By combining subroutines for generating and subsampling pseudoproxy data, performing robust statistical tests, and building interpretive tools for deciphering user results, QUANTIFA is uniquely capable of both exploring the influence of high-frequency climate signals over IFA distributional shape and providing a statistical basis for establishing IFA-Mg/Ca records of past climate variability.

In a series of model application exercises, we reaffirm several aspects of Q-Q analysis reported in earlier IFA reconstructions (Ford et al., 2015; White et al., 2018; Thirumalai et al., 2019; White and Ravelo, 2020; Rustic et al., 2020). First, we demonstrate that IFA sample size has a weak impact on the false positive rates of extreme quantiles, suggesting that they may be viewed as reliable indicators of high-frequency climate variability, a finding that carries significant implications for paleo-ENSO reconstructions based on tail quantiles (White et al., 2018; White and Ravelo, 2020; Rustic et al., 2020). However, smaller IFA sample sizes still run the risk of underrepresenting the larger population distribution and can lead to ambiguous results, underscoring the importance of sample size considerations when reconstructing past paleotemperature distributions (Thirumalai et al., 2013). Secondly, case studies across the tropical Pacific suggest that the dominant climate signal retained by IFA populations is largely determined by the annual-to-interannual ratio of climate variability at a given location and depth, a finding consistent with results from the original INFAUNAL algorithm (Thirumalai et al., 2013). Finally, our case studies reveal that in regions where annual and interannual climate variability play equally important roles in shaping IFA population distributions (such as in the upper-mixed layer at ODP Site 849), isolating quantile behavior in the interior and the tails of paleotemperature distributions, as well as accounting for biases in shell flux to the sediments, can provide clarity in parsing a particular climate signal of interest.

Although our exercises above are restricted to the tropical Pacific, we note that QUANTIFA can be used to support IFA reconstructions in other tropical oceans. ORA-S5 datasets spanning the tropical Atlantic and Indian Oceans are available to download alongside the QUANTIFA algorithm. With these data, QUANTIFA can be leveraged to reconstruct seasonality and

interannual climate phenomena associated with those basins, such as the Atlantic Niño or the Indian Ocean Dipole. However, given evidence for strong interactions between ENSO and these other tropical modes of climate variability with different seasonal phasing (Saravanan and Chang, 2000; Li et al., 2003; Behera et al., 2006), we caution that QUANTIFA is not capable of isolating the ENSO-only component of interannual climate variability in the Atlantic or Indian Oceans. Users should therefore keep these teleconnections in mind when applying QUANTIFA to regions outside of the tropical Pacific.

It should also be emphasized that, at present, the uncertainty and interpretative framework offered in QUANTIFA is not comprehensive. For sediment samples with long temporal resolution (e.g., the Holocene and YD intervals from the Line Islands cores), QUANTIFA does not account for the influence of decadal- or centennial-scale climate oscillations that could contribute to IFA population variability. Moreover, uncertainties related to migrations in the mean calcification depth of foraminifera, as well as post-depositional effects such as bioturbation, are not simulated here. However, we anticipate future additions to QUANTIFA's core code that would provide more comprehensive constraints on the non-environmental influences regulating IFA variability.

Overall, QUANTIFA represents a potentially valuable computational tool that can be easily implemented to provide a strong statistical foundation for future IFA-based reconstructions.

Acknowledgements

The authors would like to acknowledge the three anonymous reviewers and editor-in-chief Matthew Huber whose comments significantly (p < 0.05) improved the quality of this manuscript. This project was funded by National Science Foundation (NSF) Grant OCE-1701380 awarded to M.S. and student grants awarded to R.G. from both the College of Sciences at Old Dominion University and the Cushman Foundation for Foraminiferal Research. K.T. also acknowledges support from the NSF (Grant OCE-1903482) and the University of Arizona, Technology and Research Initiative Fund (TRIF). QUANTIFA is publicly available to download online from GitHub (https://github.com/rh-glaubke/QUANTIFA) or Zenodo (http://doi.org/10.5281/zenodo.4279608) alongside the underlying ORA-S5 data structures and the example datasets used in the manuscript.

References

- Behera, S. K., Luo, J. J., Masson, S., Rao, S. A., Sakuma, H., & Yamagata, T. (2006). A CGCM study on the interaction between IOD and ENSO. *Journal of Climate*, *19*(9), 1688–1705. https://doi.org/10.1175/JCLI3797.1
- Carré, M., Sachs, J. P., Purca, S., Schauer, A. J., Braconnot, P., Falcón, R. A., et al. (2014). Holocene history of ENSO variance and asymmetry in the eastern tropical Pacific. *Science (New York, N.Y.)*, 345(6200), 1045–1048. https://doi.org/10.1126/science.1252220
- Chang, P., Ji, L., Wang, B., & Li, T. (1995). Interactions between the seasonal cycle and El Nino-Southern Oscillation in an intermediate coupled ocean-atmosphere model. *Journal of the Atmospheric Sciences*, *52*(13), 2353–2372. https://doi.org/10.1175/1520-0469(1995)052<2353:ibtsca>2.0.co;2
- Chang, P., Wang, B., Li, T., & Ji, L. (1994). Interactions between the seasonal cycle and the Southern Oscillation □ Frequency entrainment and chaos in a coupled ocean □ atmosphere model. *Geophysical Research Letters*, 21(25), 2817–2820. https://doi.org/10.1029/94GL02759
- Chen, S., Hoffmann, S. S., Lund, D. C., Cobb, K. M., Emile-Geay, J., & Adkins, J. F. (2016). A high-resolution speleothem record of western equatorial Pacific rainfall: Implications for Holocene ENSO evolution. *Earth and Planetary Science Letters*, *442*, 61–71. https://doi.org/10.1016/j.epsl.2016.02.050
- Conroy, J. L., Overpeck, J. T., Cole, J. E., Shanahan, T. M., & Steinitz-Kannan, M. (2008). Holocene changes in eastern tropical Pacific climate inferred from a Galápagos lake sediment record. *Quaternary Science Reviews*, 27(11–12), 1166–1180. https://doi.org/10.1016/j.quascirev.2008.02.015
- Dolman, A. M., & Laepple, T. (2018). Sedproxy: A forward model for sediment-archived climate proxies. *Climate of the Past*, *14*(12), 1851–1868. https://doi.org/10.5194/cp-14-1851-2018
- Efron, B. (1979). Bootstrap Methods: Another Look at the Jackknife. *The Annals of Statistics*, 7(1), 1–26. https://doi.org/10.1214/aos/1176344552
- Emile-Geay, J., Cobb, K. M., Carre, M., Braconnot, P., Leloup, J., Zhou, Y., et al. (2016). Links between tropical Pacific seasonal, interannual and orbital variability during the Holocene. *Nature Geoscience*. https://doi.org/10.1038/ngeo2608
- Evans, M. N., Tolwinski-Ward, S. E., Thompson, D. M., & Anchukaitis, K. J. (2013, September 15). Applications of proxy system modeling in high resolution paleoclimatology. *Quaternary Science Reviews*. https://doi.org/10.1016/j.quascirev.2013.05.024

- Ford, H. L., Ravelo, A. C., & Polissar, P. J. (2015). Reduced El Niño-Southern Oscillation during the last glacial maximum. *Science*, *347*(6219), 255–258. https://doi.org/10.1126/science.1258437
- Ganssen, G. M., Peeters, F. J. C., Metcalfe, B., Anand, P., Jung, S. J. A., Kroon, D., & Brummer, G. J. A. (2011). Quantifying sea surface temperature ranges of the Arabian Sea for the past 20 000 years. *Climate of the Past*, 7(4), 1337–1349. https://doi.org/10.5194/cp-7-1337-2011
- Greene, C., & Thirumalai, K. (2019). It's Time to Shift Emphasis Away from Code Sharing. *Eos*, *100*(5), 16–17. https://doi.org/10.1029/2019eo116357
- Groeneveld, J., Ho, S. L., Mackensen, A., Mohtadi, M., & Laepple, T. (2019). Deciphering the Variability in Mg/Ca and Stable Oxygen Isotopes of Individual Foraminifera. *Paleoceanography and Paleoclimatology*, 34(5), 755–773. https://doi.org/10.1029/2018PA003533
- Holland, K., Branson, O., Haynes, L. L., Hönisch, B., Allen, K. A., Russell, A. D., et al. (2020). Constraining multiple controls on planktic foraminifera Mg/Ca. *Geochimica et Cosmochimica Acta*, 273, 116–136. https://doi.org/10.1016/j.gca.2020.01.015
- Jonkers, L., & Kučera, M. (2015). Global analysis of seasonality in the shell flux of extant planktonic Foraminifera. *Biogeosciences*, *12*(7), 2207–2226. https://doi.org/10.5194/bg-12-2207-2015
- Khider, D., Huerta, G., Jackson, C., Stott, L. D., & Emile-Geay, J. (2015). A Bayesian, multivariate calibration for Globigerinoides ruber Mg/Ca. *Geochemistry, Geophysics, Geosystems*, 16(9), 2916–2932. https://doi.org/10.1002/2015GC005844
- Khider, D., Stott, L. D., Emile-Geay, J., Thunell, R., & Hammond, D. E. (2011). Assessing El Niño Southern Oscillation variability during the past millennium. *Paleoceanography*, 26(3). https://doi.org/10.1029/2011PA002139
- Koutavas, A., DeMenocal, P. B., Olive, G. C., & Lynch-Stieglitz, J. (2006). Mid-Holocene El Niño-Southern Oscillation (ENSO) attenuation revealed by individual foraminifera in eastern tropical Pacific sediments. *Geology*, *34*(12), 993–996. https://doi.org/10.1130/G22810A.1
- Koutavas, A., & Joanides, S. (2012). El Niño-Southern Oscillation extrema in the Holocene and Last Glacial Maximum. *Paleoceanography*, *27*(4), 1–15. https://doi.org/10.1029/2012PA002378
- Kucera, M. (2007). Planktonic Foraminifera as Tracers of Past Oceanic Environments, Chapter 6. In C. Hillaire–Marcel & A. De Vernal (Eds.), *Developments in Marine Geology* (Vol. 1, pp. 213–262). Oxford: Elsevier B.V. https://doi.org/10.1016/S1572-5480(07)01011-1

- Leduc, G., Vidal, L., Cartapanis, O., & Bard, E. (2009). Modes of eastern equatorial Pacific thermocline variability: Implications for ENSO dynamics over the last glacial period. *Paleoceanography*, 24(3), 1–14. https://doi.org/10.1029/2008PA001701
- Li, T., Wang, B., Chang, C. P., & Zhang, Y. (2003). A theory for the Indian Ocean dipole-zonal mode. *Journal of the Atmospheric Sciences*, 60(17), 2119–2135. https://doi.org/10.1175/1520-0469(2003)060<2119:ATFTIO>2.0.CO;2
- Liu, Z. (2002). A simple model study of ENSO suppression by external periodic forcing. *Journal of Climate*, *15*(9), 1088–1098. https://doi.org/10.1175/1520-0442(2002)015<1088:ASMSOE>2.0.CO;2
- Liu, S., Jiang, D., & Lang, X. (2020). The Weakening and Eastward Movement of ENSO Impacts during the Last Glacial Maximum. *Journal of Climate*, *33*(13), 5507–5526. https://doi.org/10.1175/jcli-d-19-0728.1
- Liu, Z., Lu, Z., Wen, X., Otto-Bliesner, B. L., Timmermann, A., & Cobb, K. M. (2014). Evolution and forcing mechanisms of El Niño over the past 21,000 years. *Nature*, 515(7528), 550–553. https://doi.org/10.1038/nature13963
- Lodder, R. A., & Hieftje, G. M. (1988). Quantile analysis: A method for characterizing data distributions. *Applied Spectroscopy*, 42(8), 1512–1520. https://doi.org/10.1366/0003702884429724
- Lu, Z., Liu, Z., & Zhu, J. (2016). Abrupt intensification of ENSO forced by deglacial ice-sheet retreat in CCSM3. *Climate Dynamics*, 46(5–6), 1877–1891. https://doi.org/10.1007/s00382-015-2681-3
- McGregor, H. V, & Gagan, M. K. (2004). Western Pacific coral \$δ\$18O records of anomalous Holocene variability in the El Niño-Southern Oscillation. *Geophysical Research Letters*, 31(11). https://doi.org/10.1029/2004GL019972
- Moy, C. M., Seltzer, G. O., Rodbell, D. T., & Anderson, D. M. (2002). Variability of El Niño/Southern Oscillation activity at millennial timescales during the Holocene epoch. *Nature*, 420(6912), 162–165. https://doi.org/10.1038/nature01194
- Rein, B., Lückge, A., Reinhardt, L., Sirocko, F., Wolf, A., & Dullo, W. C. (2005). El Niño variability off Peru during the last 20,000 years. *Paleoceanography*, 20(4). https://doi.org/10.1029/2004PA001099
- Rodbell, D. T., Seltzer, G. O., Anderson, D. M., Abbott, M. B., Enfield, D. B., & Newman, J. H. (1999). An ~15,000-year record of El Nino-driven alluviation in Southwestern Ecuador. *Science*, 283(5401), 516–520. https://doi.org/10.1126/science.283.5401.516

- Rustic, G. T., Polissar, P. J., Ravelo, A. C., & White, S. M. (2020). Modulation of late Pleistocene ENSO strength by the tropical Pacific thermocline. *Nature Communications*, *11*(1), 5377. https://doi.org/10.1038/s41467-020-19161-6
- Sadekov, A. Y., Ganeshram, R., Pichevin, L., Berdin, R., McClymont, E., Elderfield, H., & Tudhope, A. W. (2013). Palaeoclimate reconstructions reveal a strong link between El niñosouthern oscillation and tropical pacific mean state. *Nature Communications*, *4*, 1–8. https://doi.org/10.1038/ncomms3692
- Saravanan, R., & Chang, P. (2000). Interaction between tropical Atlantic variability and El Nino-Southern Oscillation. *Journal of Climate*, *13*(13), 2177–2194. https://doi.org/10.1175/1520-0442(2000)013<2177:IBTAVA>2.0.CO;2
- Schmitt, A., Elliot, M., Thirumalai, K., La, C., Bassinot, F., Petersen, J., et al. (2019). Single foraminifera Mg/Ca analyses of past glacial-interglacial temperatures derived from G. ruber sensu stricto and sensu lato morphotypes. *Chemical Geology*, *511*, 510–520. https://doi.org/10.1016/j.chemgeo.2018.11.007
- Scroxton, N., Bonham, S. G., Rickaby, R. E. M., Lawrence, S. H. F., Hermoso, M., & Haywood, A. M. (2011). Persistent El Niño-Southern Oscillation variation during the Pliocene Epoch. *Paleoceanography*, 26(2), n/a-n/a. https://doi.org/10.1029/2010PA002097
- Thirumalai, K., DiNezio, P. N., Tierney, J. E., Puy, M., & Mohtadi, M. (2019). An El Niño Mode in the Glacial Indian Ocean? *Paleoceanography and Paleoclimatology*, *34*(8), 1316–1327. https://doi.org/10.1029/2019pa003669
- Thirumalai, K., Partin, J. W., Jackson, C. S., & Quinn, T. M. (2013). Statistical constraints on El Niño Southern Oscillation reconstructions using individual foraminifera: A sensitivity analysis. *Paleoceanography*, 28(3), 401–412. https://doi.org/10.1002/palo.20037
- Thunell, R. C., & Reynolds, L. A. (1984). Sedimentation of Planktonic Foraminifera: Seasonal Changes in Species Flux in the Panama Basin. *Micropaleontology*, *30*(3), 243–262. https://doi.org/10.2307/1485688
- Tierney, J. E., Malevich, S. B., Gray, W., Vetter, L., & Thirumalai, K. (2019). Bayesian Calibration of the Mg/Ca Paleothermometer in Planktic Foraminifera. *Paleoceanography and Paleoclimatology*, *34*(12), 2005–2030. https://doi.org/10.1029/2019PA003744
- Timmermann, A., Okumura, Y., An, S. I., Clement, A., Dong, B., Guilyardi, E., et al. (2007). The influence of a weakening of the Atlantic meridional overturning circulation on ENSO. *Journal of Climate*, 20(19), 4899–4919. https://doi.org/10.1175/JCLI4283.1
- Vetter, L., Spero, H. J., Eggins, S. M., Williams, C., & Flower, B. P. (2017). Oxygen isotope geochemistry of Laurentide ice-sheet meltwater across Termination I. *Quaternary Science Reviews*, 178, 102–117. https://doi.org/10.1016/j.quascirev.2017.10.007

- Wallace, J. M., Mitchell, T. P., & Deser, C. (1989). The Influence of Sea-Surface Temperature on Surface Wind in the Eastern Equatorial Pacific: Seasonal and Interannual Variability. *Journal of Climate*, 2(12), 1492–1499. https://doi.org/10.1175/1520-0442(1989)002<1492:tiosst>2.0.co;2
- Wang, C., & Fiedler, P. C. (2006). ENSO variability and the eastern tropical Pacific: A review. *Progress in Oceanography*, 69(2–4), 239–266. https://doi.org/10.1016/j.pocean.2006.03.004
- Wang, W., & McPhaden, M. J. (2000). The surface-layer heat balance in the Equatorial Pacific Ocean Part II: Interannual variability. *Journal of Physical Oceanography*, *30*(11), 2989–3008. https://doi.org/10.1175/1520-0485(2001)031<2989:TSLHBI>2.0.CO;2
- White, S. M., & Ravelo, A. C. (2020). Dampened El Niño in the early Pliocene warm period. *Geophysical Research Letters*, 47(4), 1–10. https://doi.org/10.1029/2019gl085504
- White, S. M., Ravelo, A. C., & Polissar, P. J. (2018). Dampened El Niño in the Early and Mid-Holocene due to Insolation-Forced Warming/Deepening of the Thermocline. *Geophysical Research Letters*, 45(1), 316–326. https://doi.org/10.1002/2017GL075433
- Wit, J. C., Reichart, G. J., A Jung, S. J., & Kroon, D. (2010). Approaches to unravel seasonality in sea surface temperatures using paired single-specimen foraminiferal δ18O and Mg/Ca analyses. *Paleoceanography*, 25(4), n/a-n/a. https://doi.org/10.1029/2009PA001857
- Zuo, H., Balmaseda, M. A., Tietsche, S., Mogensen, K., & Mayer, M. (2019). The ECMWF operational ensemble reanalysis–analysis system for ocean and sea ice: a description of the system and assessment. *Ocean Science*, *15*(3), 779–808. https://doi.org/10.5194/os-15-779-2019

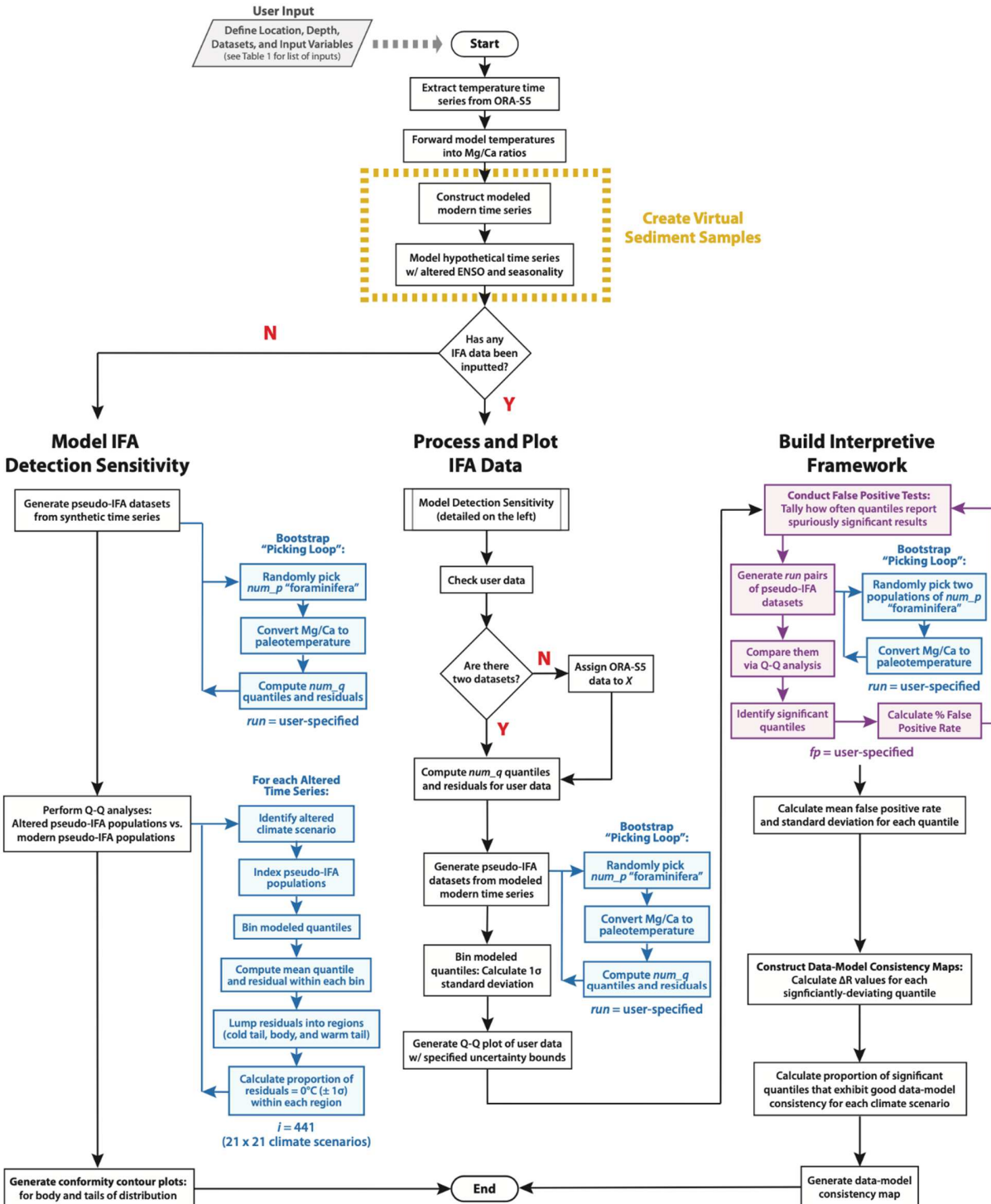


Figure 1. A flowchart detailing QUANTIFA's order of operations. Blue and purple regions represent iterative subroutines built within the algorithm (purple used where loops are nested). See Table 1 for description of variable names (italicized).

Input Parameters for QUANTIFA	1	
Parameter	Variable	Description
Individual Foraminiferal Data		
Reference Population	X	IFA Population to be plotted along the X-axis [Omit if performing sensitivity analysis]
Comparison Population	Y	IFA Population to be plotted along the Y-axis [Omit if performing sensitivity analysis]
Reanalysis Data		
ORA-S5 Data Structure		A subset of Ocean Reanalysis System 5 potential temperature data (available for download).
Core Location	-	
Latitude	lat	Latitude of the core location (XX.5°)
Longitude	lon	Longitude of the core location (XX°)
Depth	dep	Mean calcification depth for foraminiferal species of interest
Calibration Equation		
Calibration Equation	eqn	Select from a bank of preloaded Mg/Ca-T calibrations (see Table S1) or program your own.
Dissolution Correction	D	For preloaded calibration equations that incorporate dissolution correction terms, the term (in km core depth, [CO ₃ ²⁻], or any other variable) can be entered here.
Initializing Conditions		
Number of Picked "Foraminifera"	num_p	No. of individuals in pseudo-IFA populations "picked" by QUANTIFA.
Number of Quantiles	num_q	No. of quantiles computed from pseudo-IFA data (ideally $num_q < nump_p$).
Seasonal Weighting	seas	Months weighted in QUANTIFA's picking algorithm (1 $-$ 12 by default).
Pseudoproxy Time Series Length	tsl	Length (in yrs) of the pseudoproxy time series (equal to sampling resolution if running IFA data)
Model Realizations	run	No. of pseudo-IFA populations (and, by extension, Q-Q realizations) generated by QUANTIFA.
False Positive Rate Exercises	fp	No. of false positive rate exercises (recommended: $100 \text{ for } run = 1000 - 5000$)
Confidence Level	cl	Confidence level for uncertainty envelopes (85%, 90%, 95%, or 99%)
Analytical Error	anerr	Analytical uncertainty (in mmol/mol) from IFA measurements (choose a generic value, e.g., 0.1 mmol/mol, if running sensitivity tests).
Calibration Error	calerr	Error (in °C) for the selected calibration equation. [OPTIONAL]

 Table 1. Input parameters for QUANTIFA.

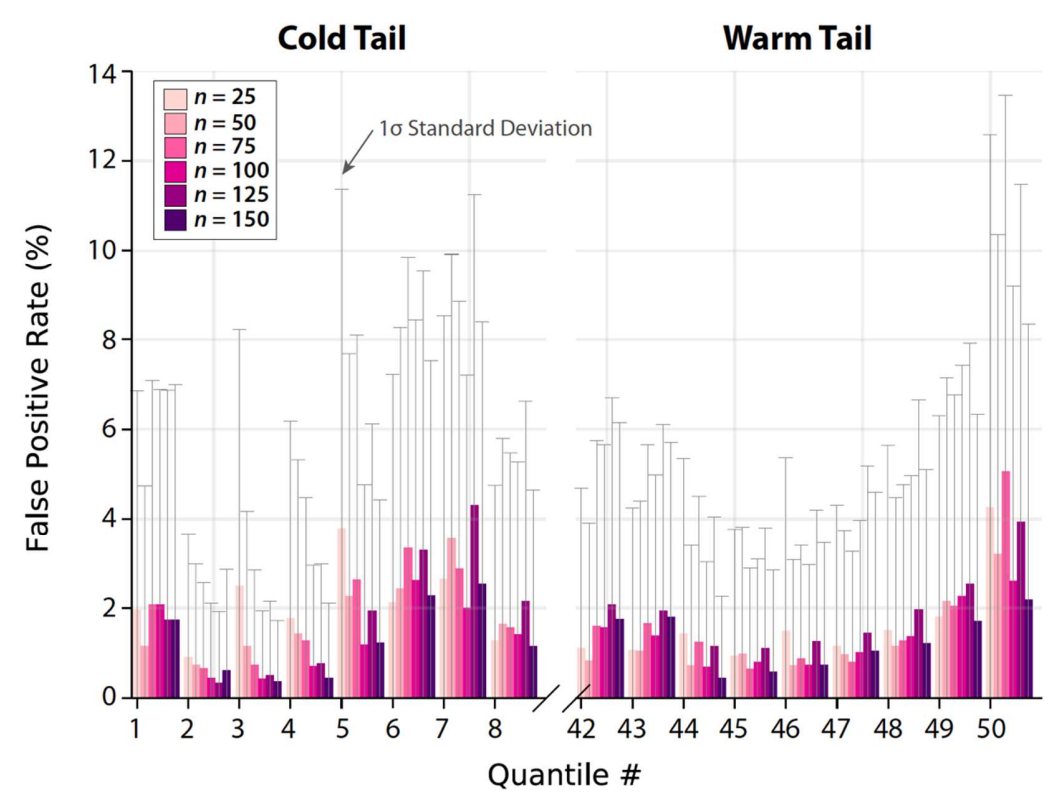


Figure 2. Average false positive rates for extreme quantiles in the tails of pseudo-IFA populations from the Niño 3.4 region under variable IFA sample sizes. Mean and standard deviation (1σ) computed by averaging false positive rates across 100 model exercises (each with 5,000 model realizations). Note that a false positive result reports a significant difference between two pseudo-IFA distributions when both are known to have come from the same population distribution.

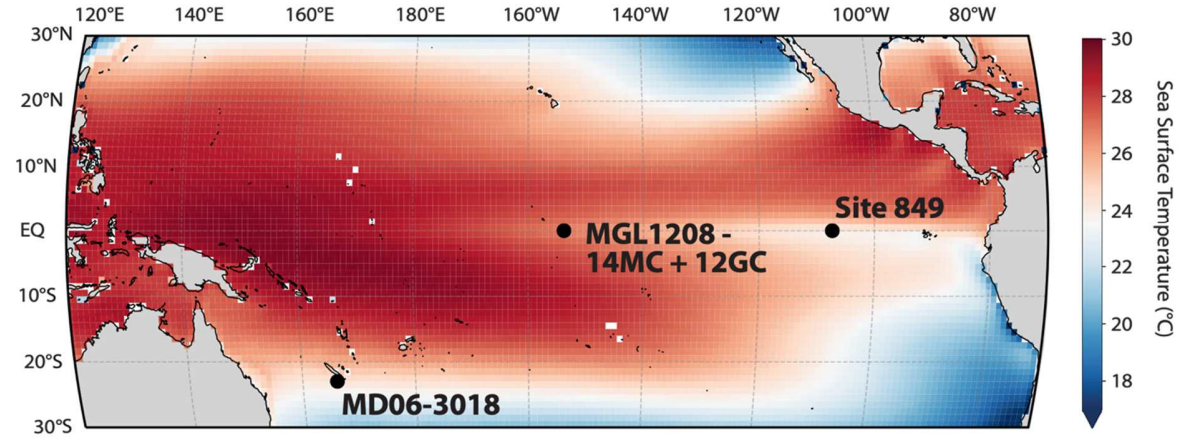
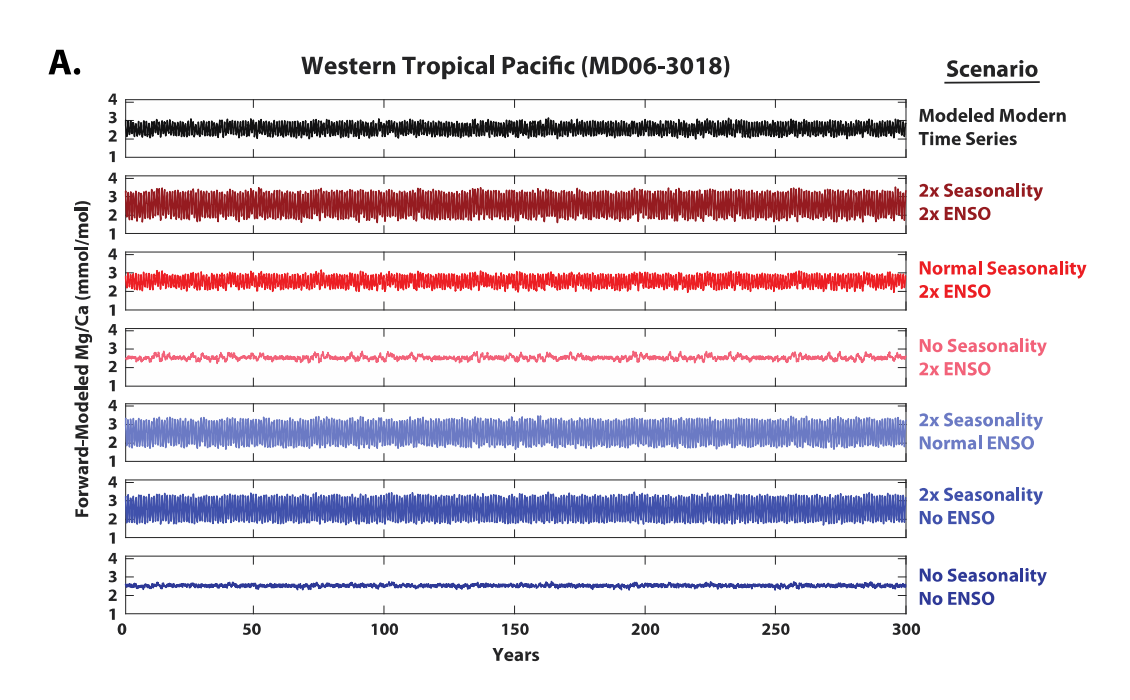


Figure 3. Core locations for core MD06-3018 (23°00'S, 166°09'E; 2470 m) (Schmitt et al., 2019), cores MGL1208-14MC and MGL1208-12GC (0°13'S, 155°58'W, 3049 m) (White et al., 2018), and ODP Site 849 (0°11'N, 110°31'W, 3851 m) (Ford et al., 2015) plotted atop mean sea surface temperatures from ORA-S5 (1958 – 2018). Latitudinal and longitudinal bounds of the map correspond to the lateral domain of the ORA-S5 tropical Pacific dataset.



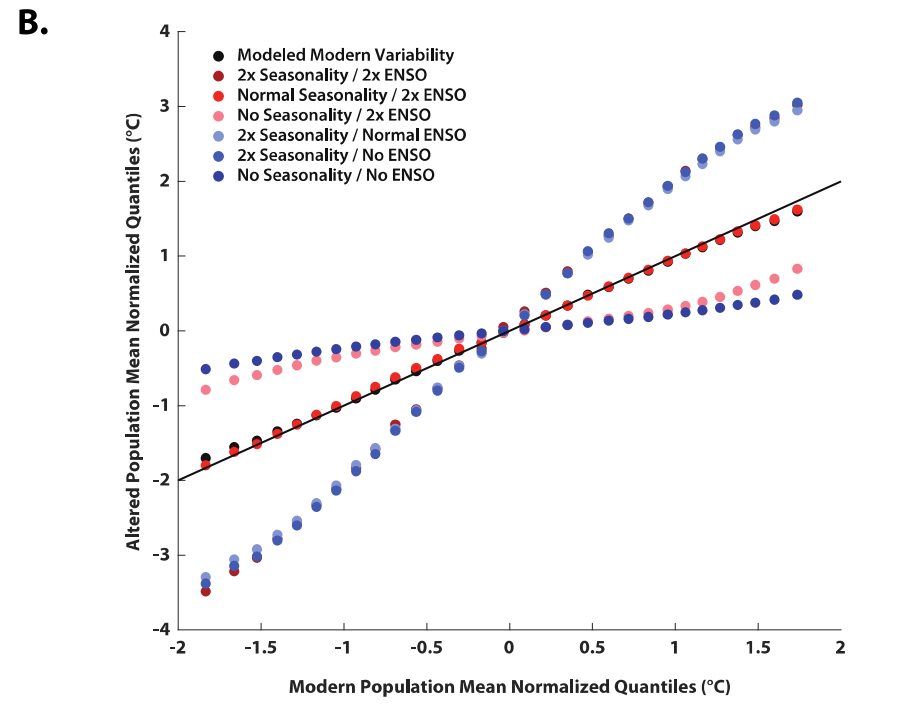


Figure 4. Modeled results from the core site of MD06-3018 in the western Pacific. (A) Pseudoproxy time series from select paleoclimate scenarios (listed to the right of the time series) and (B) their associated expression in QQ space when compared against modeled modern climate variability.

Western Tropical Pacific (MD06-3018)

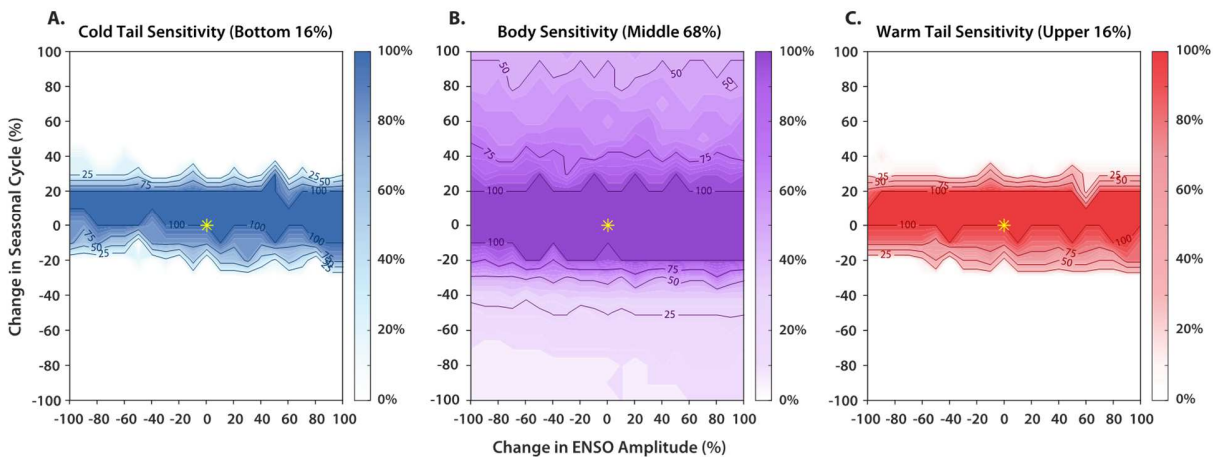


Figure 5. Conformity contour plots (%) for theoretical paleotemperature distributions from G. ruber at the site of MD06-3018 (depth = 40 m; see supplemental information). Contours report the proportion of quantiles within the (A) cold tail, (B) interior, and (C) warm tail that conform to the modeled modern time series (i.e., lie within $\pm 1\sigma$ from the 1:1 line). The yellow star represents modern climate variability (0% change in ENSO and seasonal cycle amplitude).

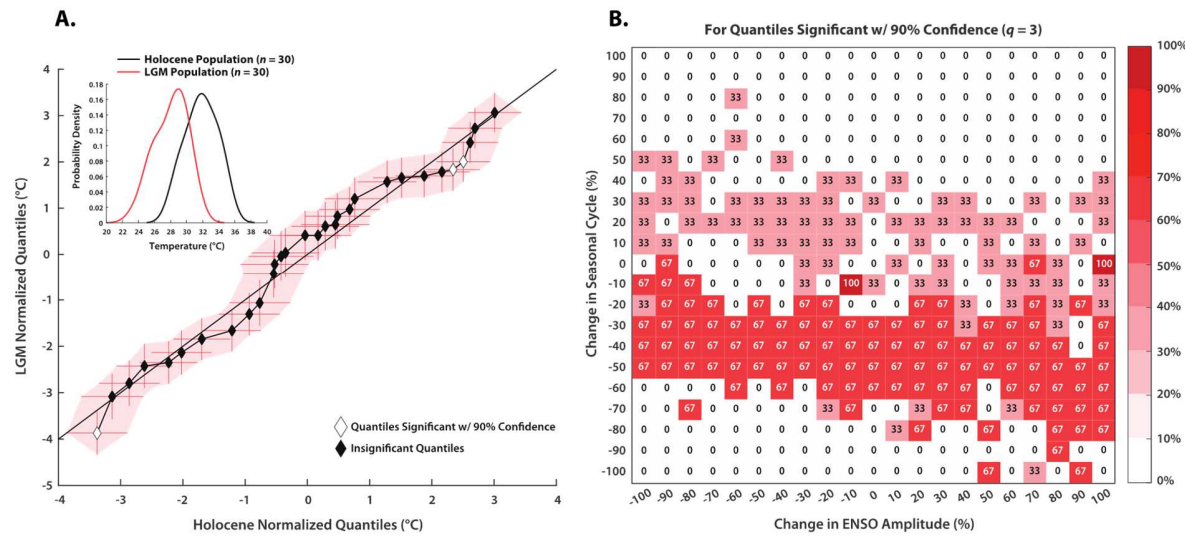
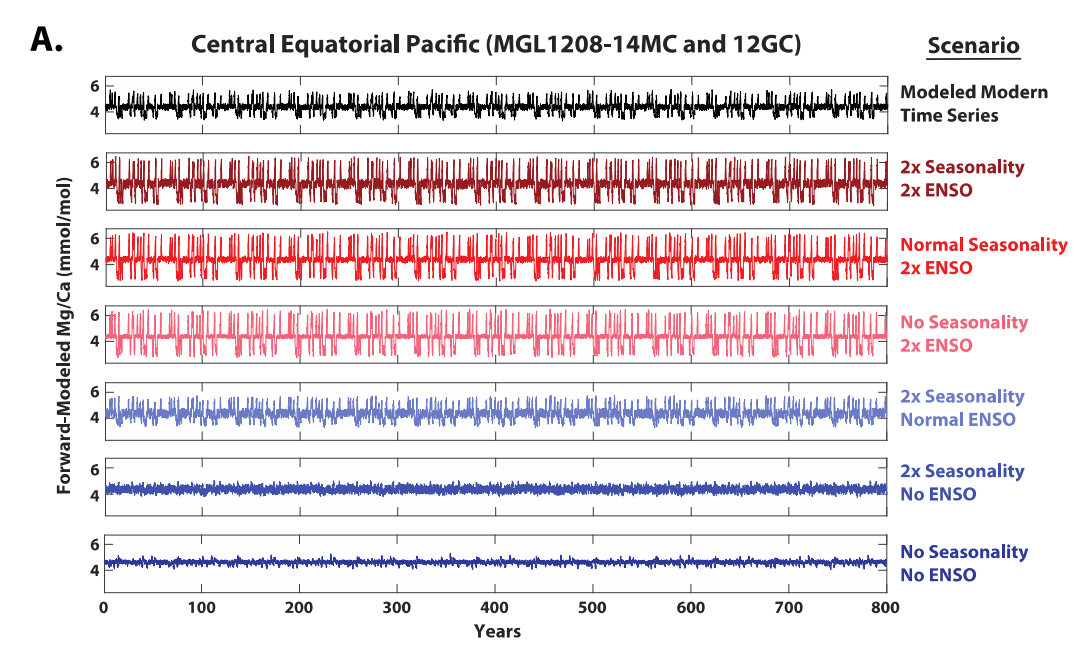


Figure 6. IFA results from MD06-3018. (A) A Q-Q plot comparing the normalized quantiles of the LGM population against the normalized quantiles of the Holocene population. X and Y error bars and the associated red enveloped represent 90% confidence bounds in both dimensions. Significant quantiles are indicated by the colored diamonds (see legend in the lower right corner). Inset shows smoothed kernel density functions for the Holocene (black) and LGM (red) populations. (B) A heat map displaying the proportion of significant quantiles that exhibit good data-model agreement for each hypothetical climate scenario (proportions calculated from total significant quantiles, q).



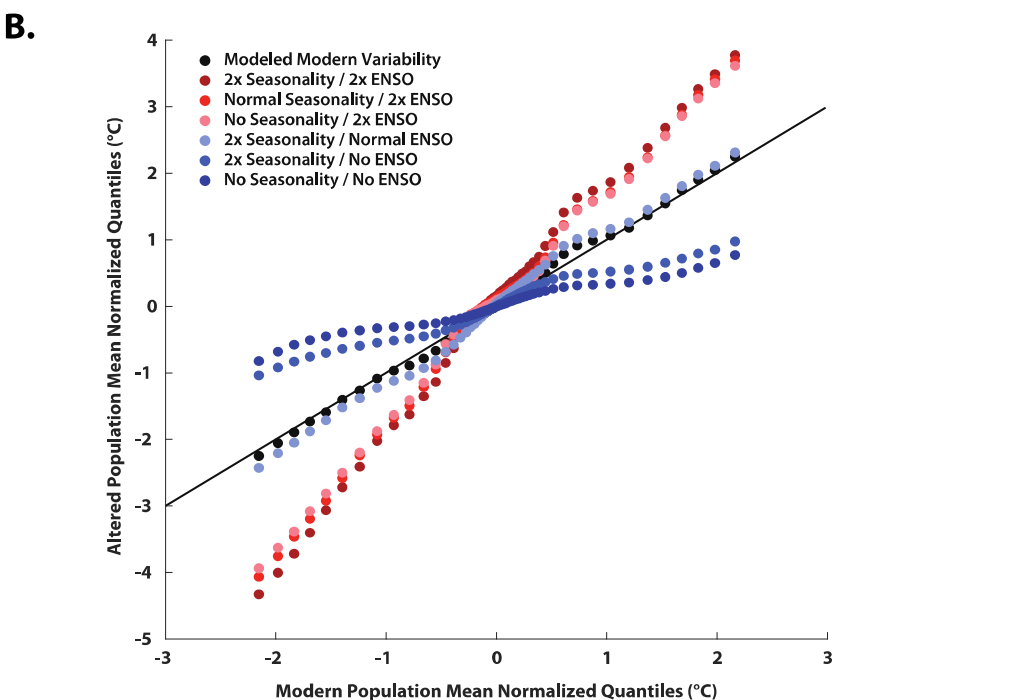


Figure 7. Modeled results from the core site of MGL1208-14MC and 12GC in the central equatorial Pacific. (A) Pseudoproxy time series from select paleoclimate scenarios (listed to the right of the time series) and (B) their associated expression in QQ space when compared against modeled modern climate variability.

Central Equatorial Pacific (MGL1208-14MC and 12GC)

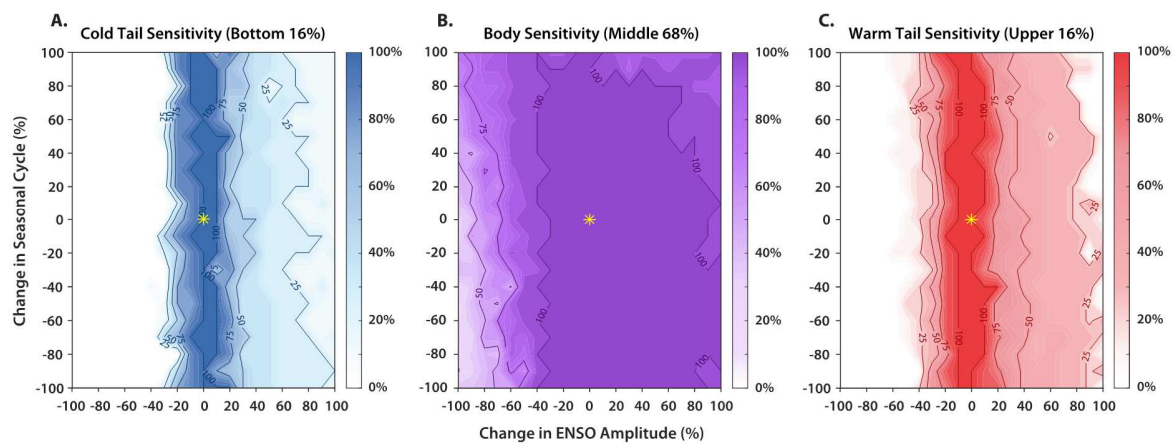


Figure 8. Conformity contour plots (%) for theoretical paleotemperature distributions from T. sacculifer populations at cores 14MC and 12GC in the central equatorial Pacific (depth = 58 m; see supplemental information). Contours report the proportion of quantiles within the (A) cold tail, (B) interior, and (C) warm tail that conform to the modeled modern time series (i.e., lie within $\pm 1\sigma$ from the 1:1 line). The yellow star represents modern climate variability (0% change in ENSO and seasonal cycle amplitude). Note the dramatic difference in the structure of the contours relative to the mixed layer of the western tropical Pacific.

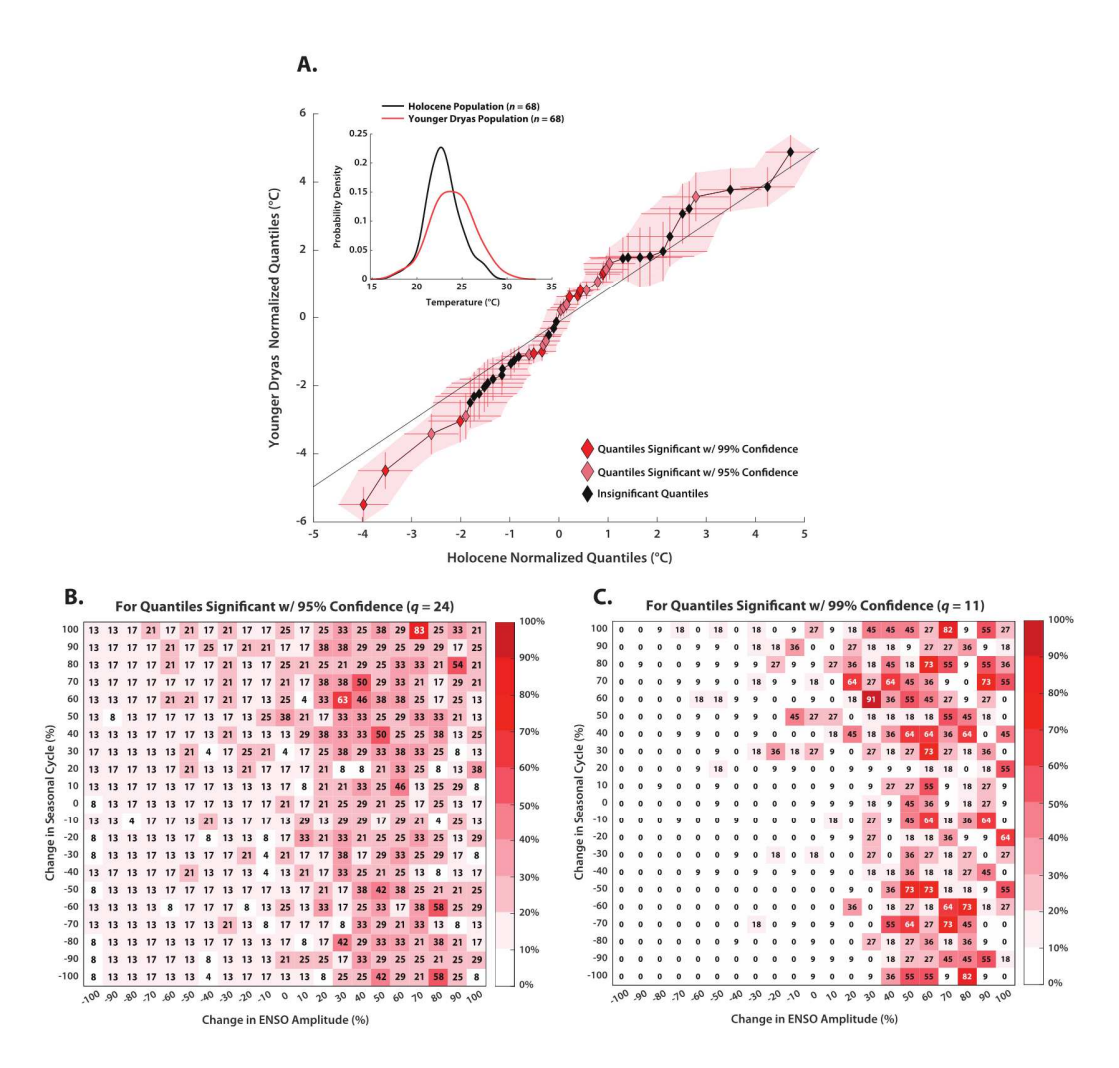
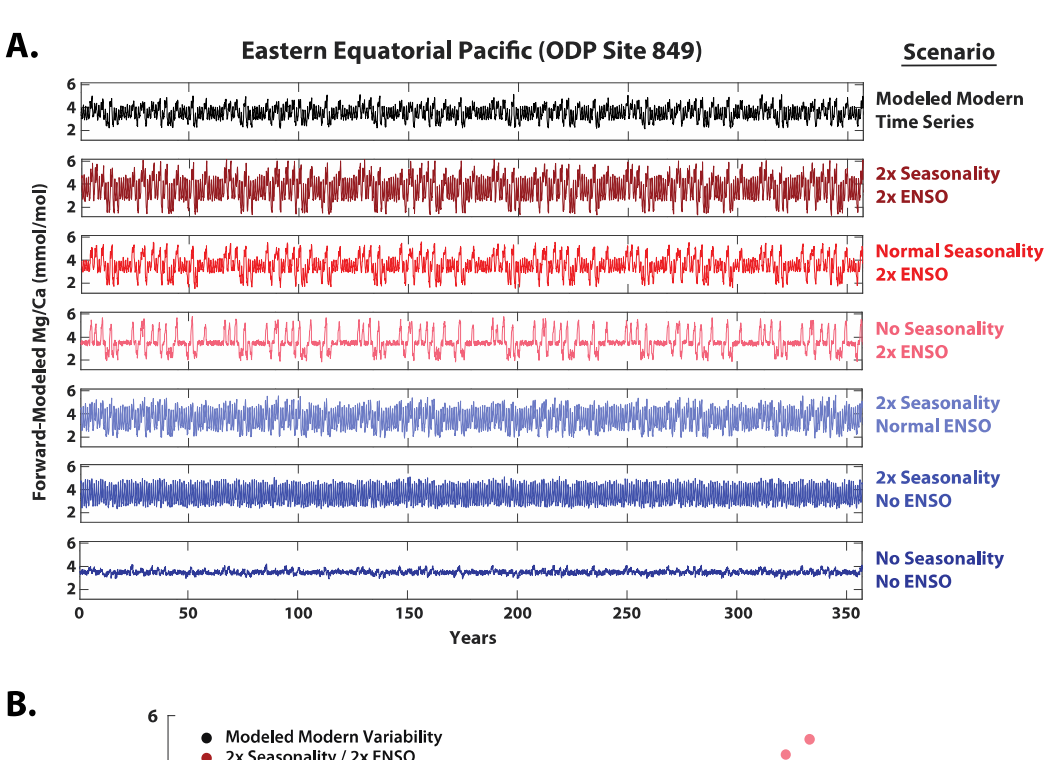


Figure 9. IFA results from cores 14MC and 12GC. (A) A Q-Q plot comparing the normalized quantiles of the YD population against the normalized quantiles of the Holocene population. X and Y error bars and the associated red enveloped represent 95% confidence bounds in both dimensions, although quantiles significant at greater levels of confidence are indicated by the colored diamonds (see legend in the lower right corner). Inset shows smoothed kernel density functions for the Holocene (black) and YD (red) populations. Q-Q results are accompanied by data-model consistency maps displaying the proportion of quantiles significant at (B) 95% and (C) 99% confidence that exhibit good data-model agreement for each hypothetical climate scenario (proportions calculated from total significant quantiles, q).



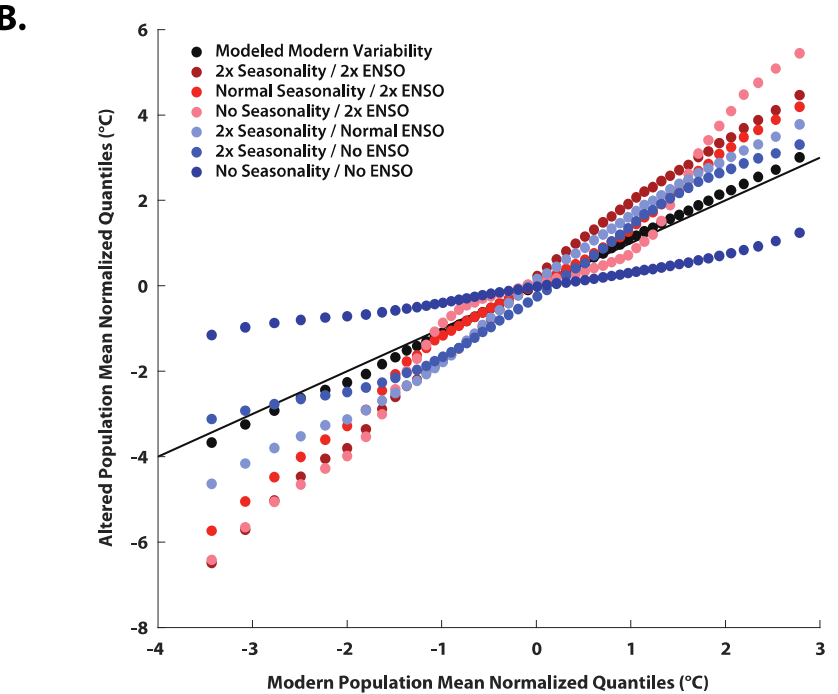


Figure 10. Modeled results from the core site of ODP Site 849 in the EEP. (A) Pseudoproxy time series from select paleoclimate scenarios (listed to the right of the time series) and (B) their associated expression in QQ space when compared against modeled modern climate variability.

Eastern Equatorial Pacific (ODP Site 849)

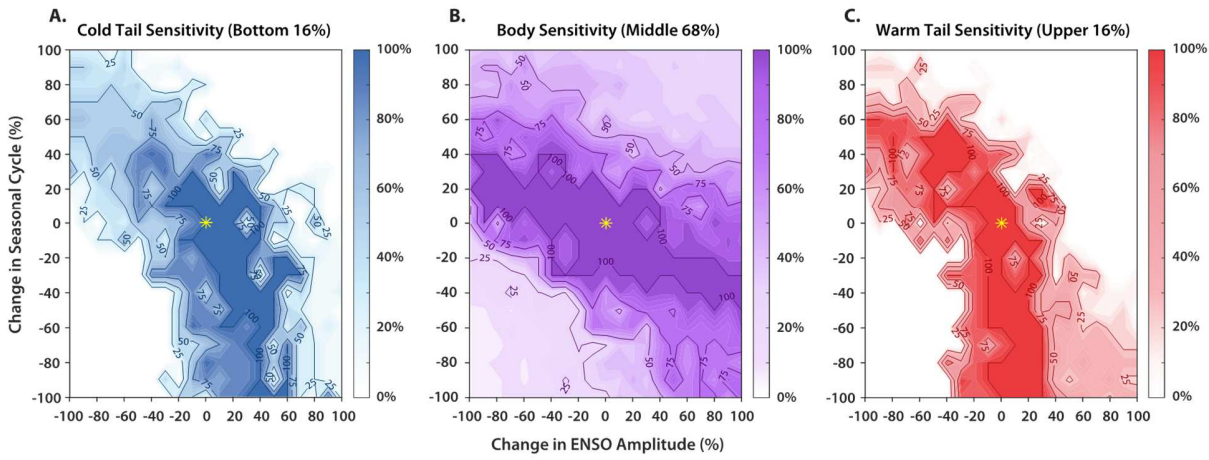
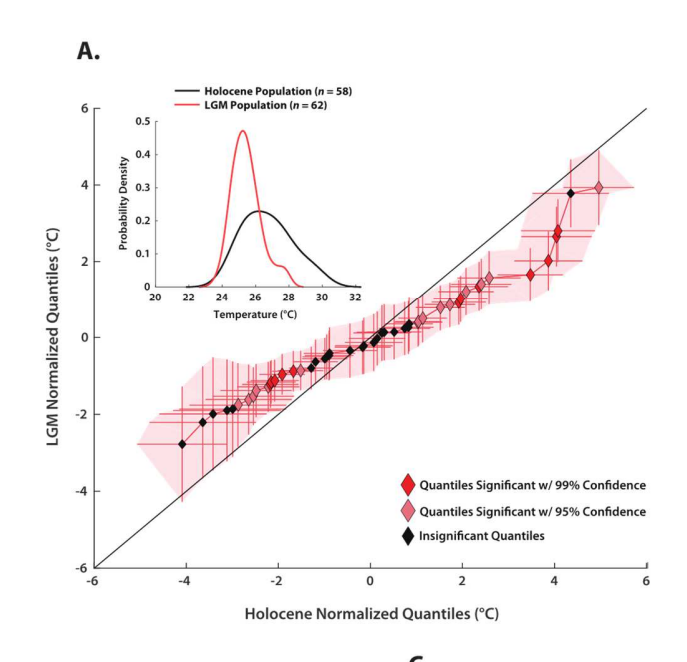


Figure 11. Conformity contour plots (%) for theoretical paleotemperature distributions from T. sacculifer populations at ODP Site 849 (depth = 15 m; see supplemental information). Contours report the proportion of quantiles within the (A) cold tail, (B) interior, and (C) warm tail that conform to the modeled modern time series (i.e., lie within $\pm 1\sigma$ from the 1:1 line). The yellow star represents modern climate variability (0% change in ENSO and seasonal cycle amplitude). The diagonal structure exhibited by the conformity contours suggests a mixed influence of annual and interannual climate variability.



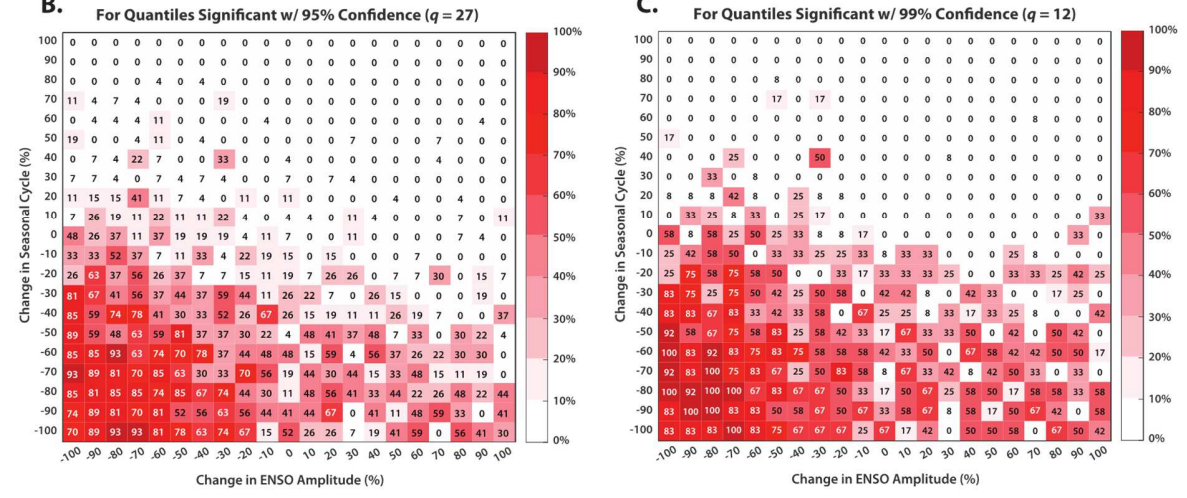
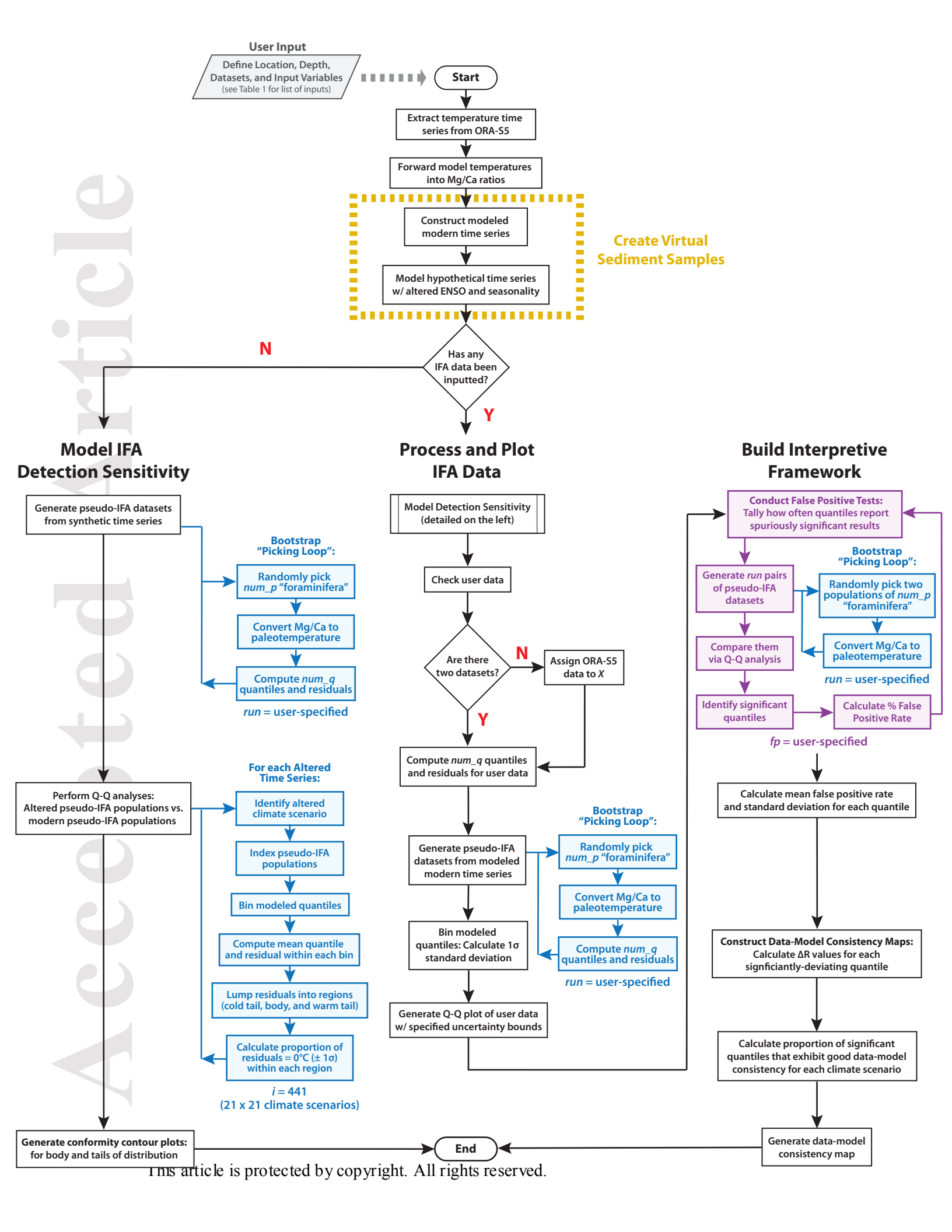
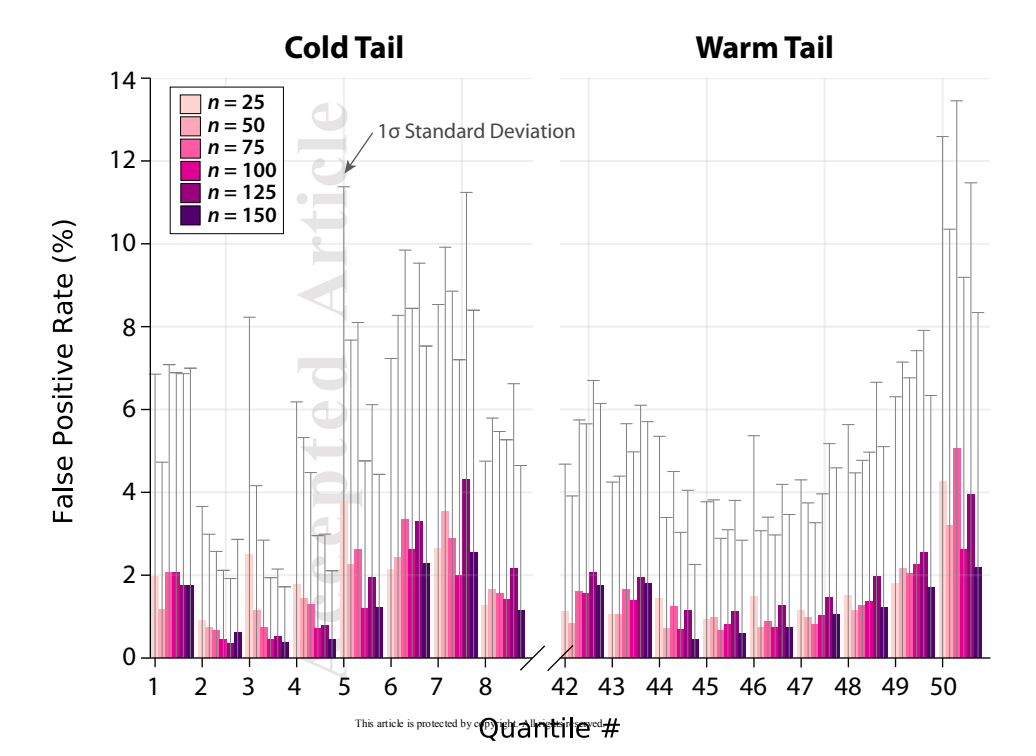
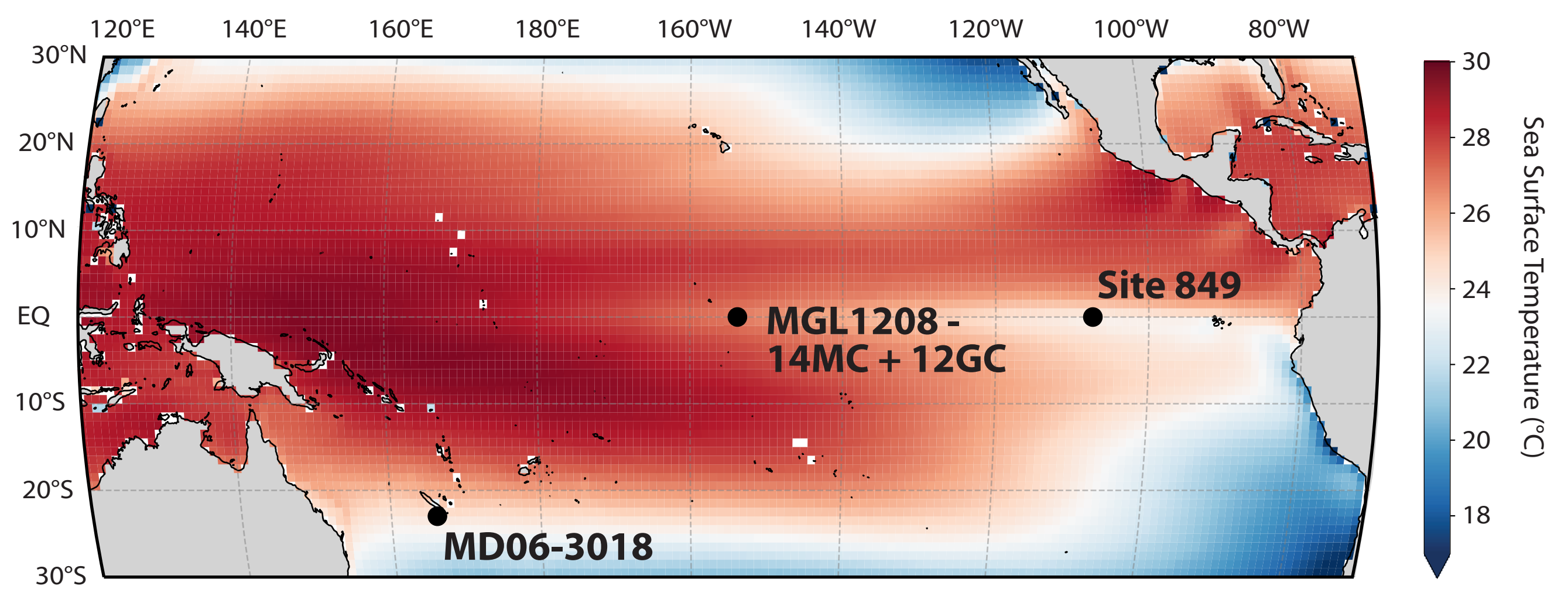
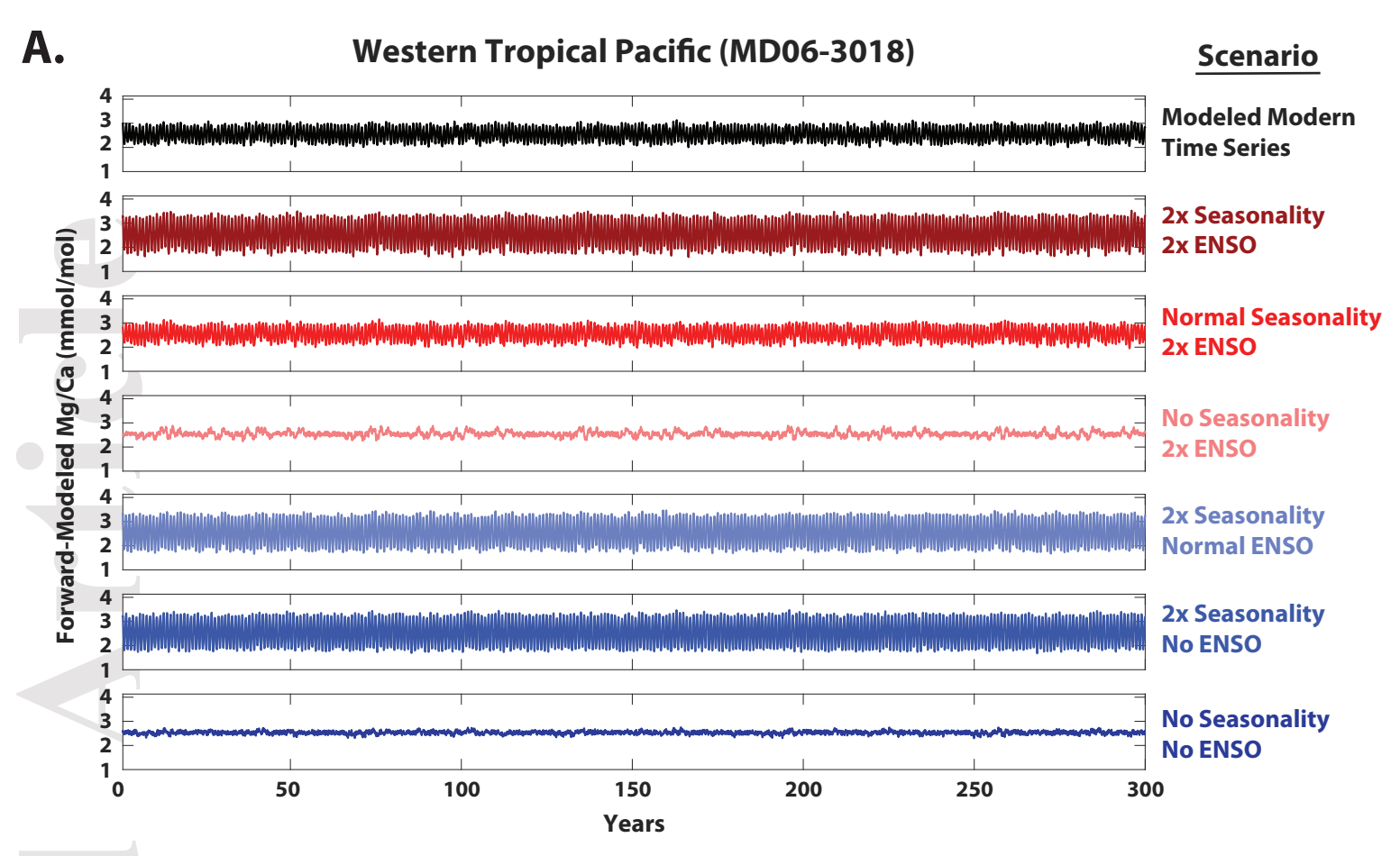


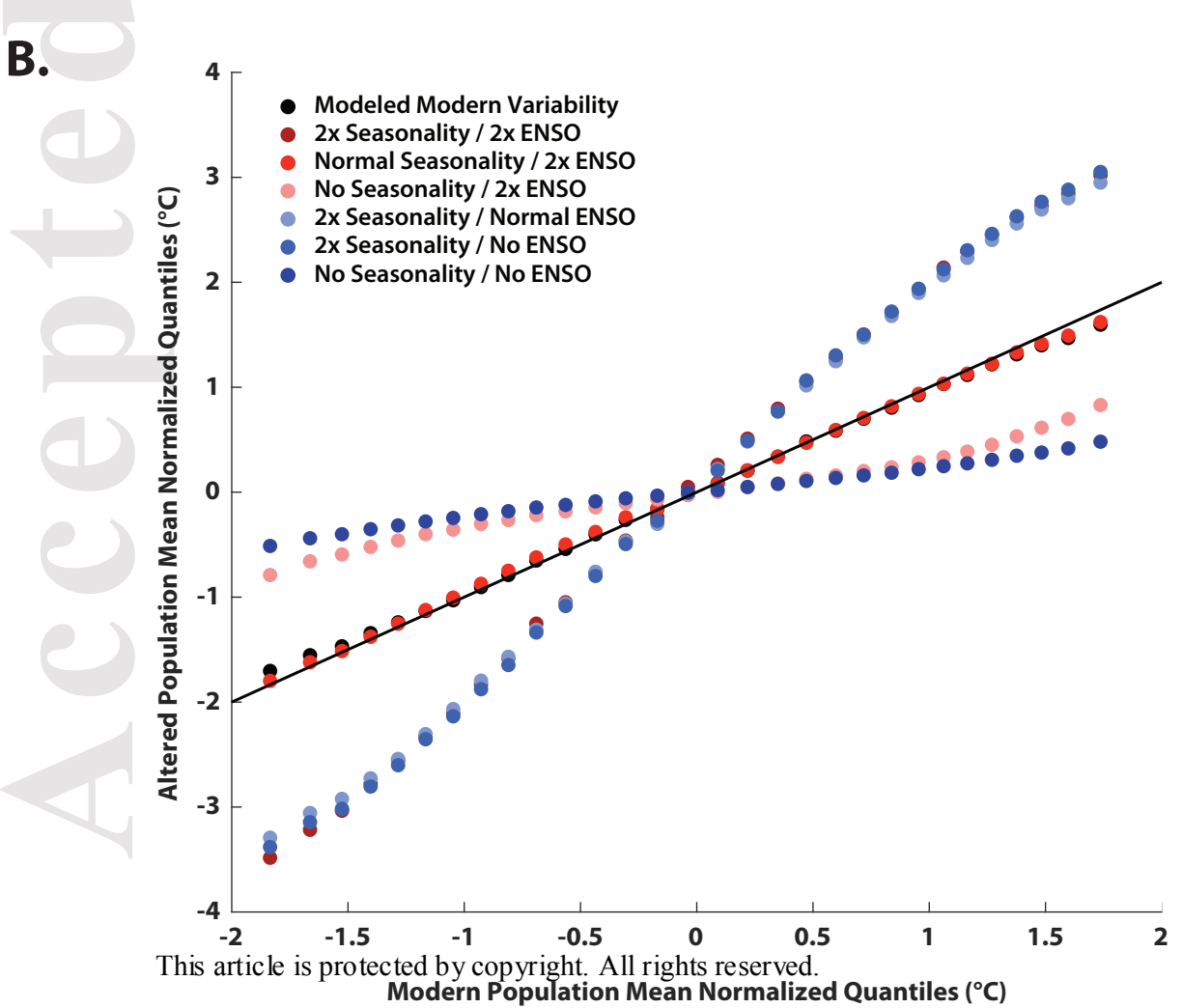
Figure 12. IFA results from ODP Site 849. (A) A Q-Q plot comparing the normalized quantiles of the LGM population against the normalized quantiles of the Holocene population. X and Y error bars and the associated red enveloped represent 95% confidence bounds in both dimensions, although quantiles significant at greater levels of confidence are indicated by the colored diamonds (see legend in the lower right corner). Inset shows smoothed kernel density functions for the Holocene (black) and LGM (red) populations. Q-Q results are accompanied by heat maps displaying the proportion of quantiles significant at (B) 95% and (C) 99% confidence that exhibit good data-model agreement for each hypothetical climate scenario (proportions calculated from total significant quantiles, *q*).



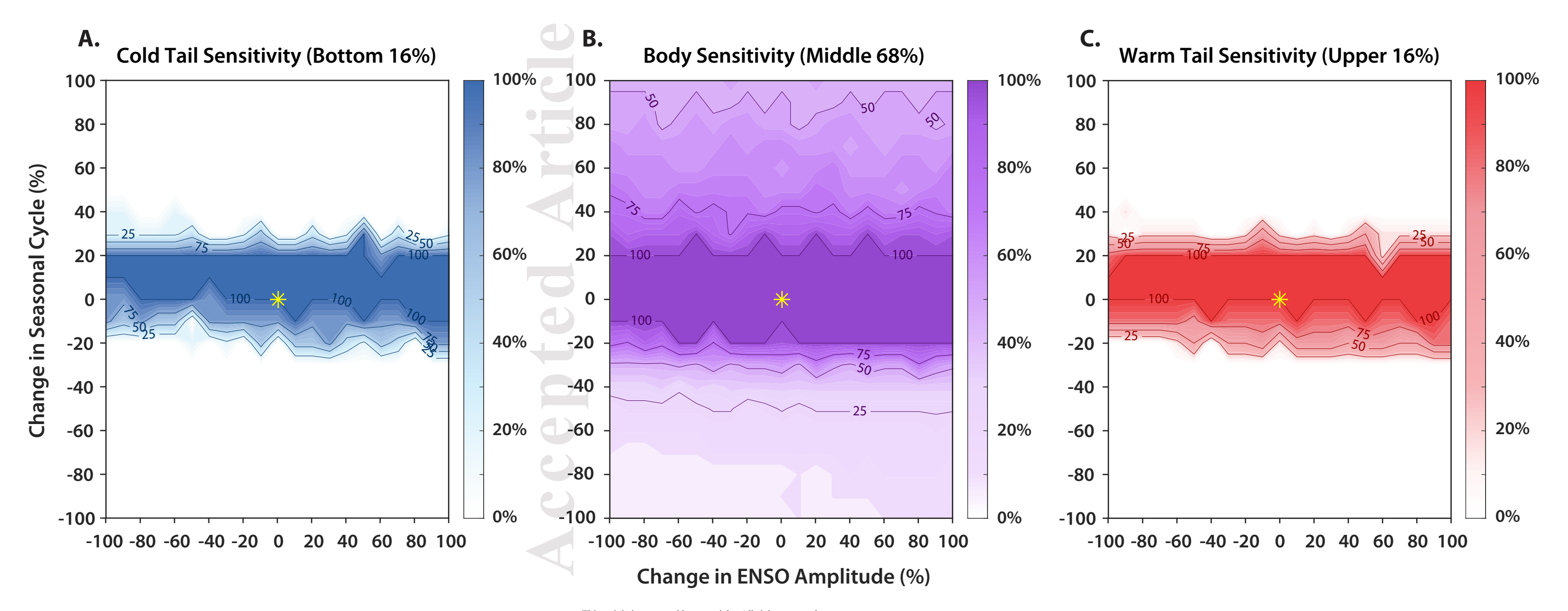


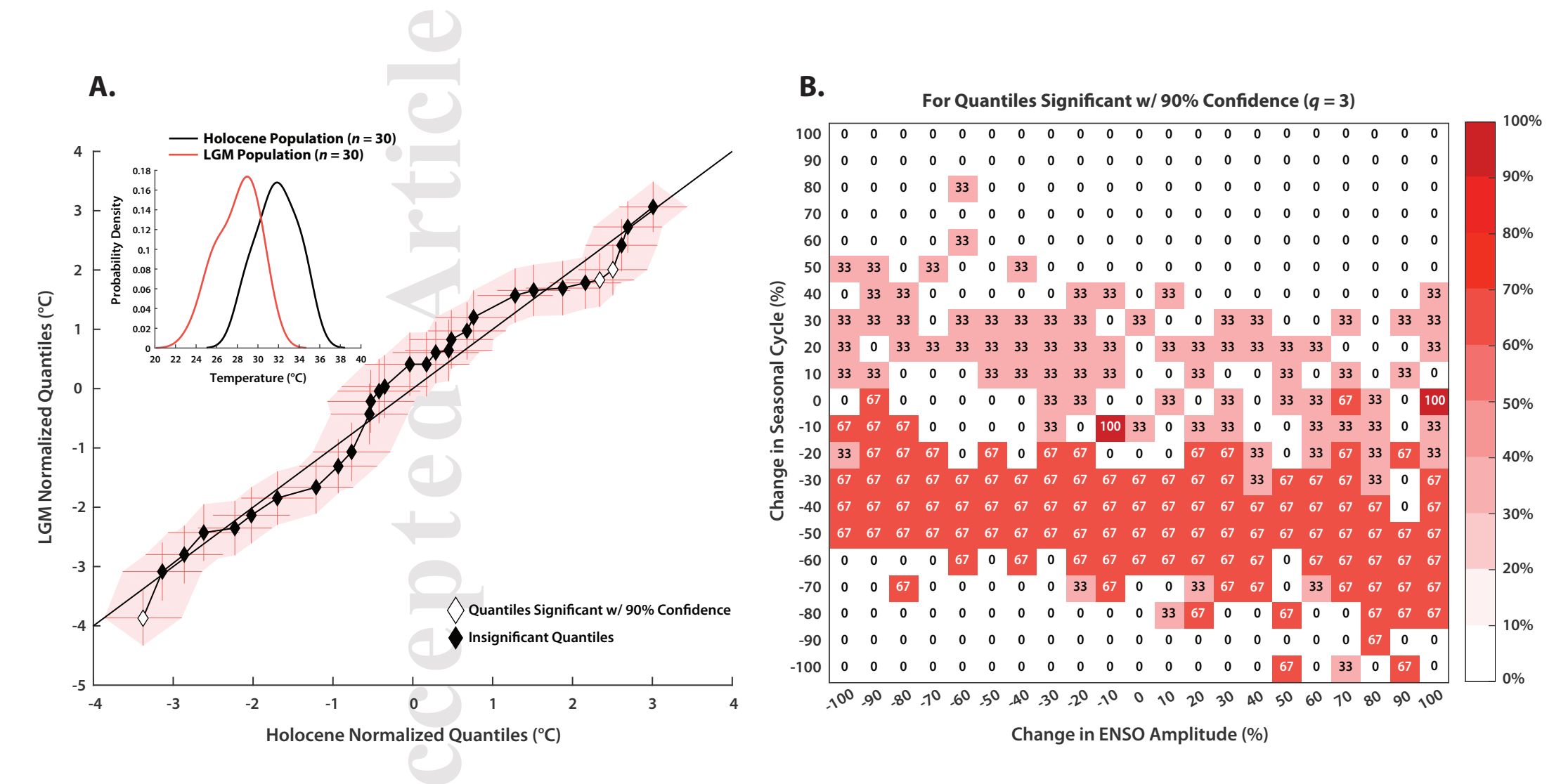


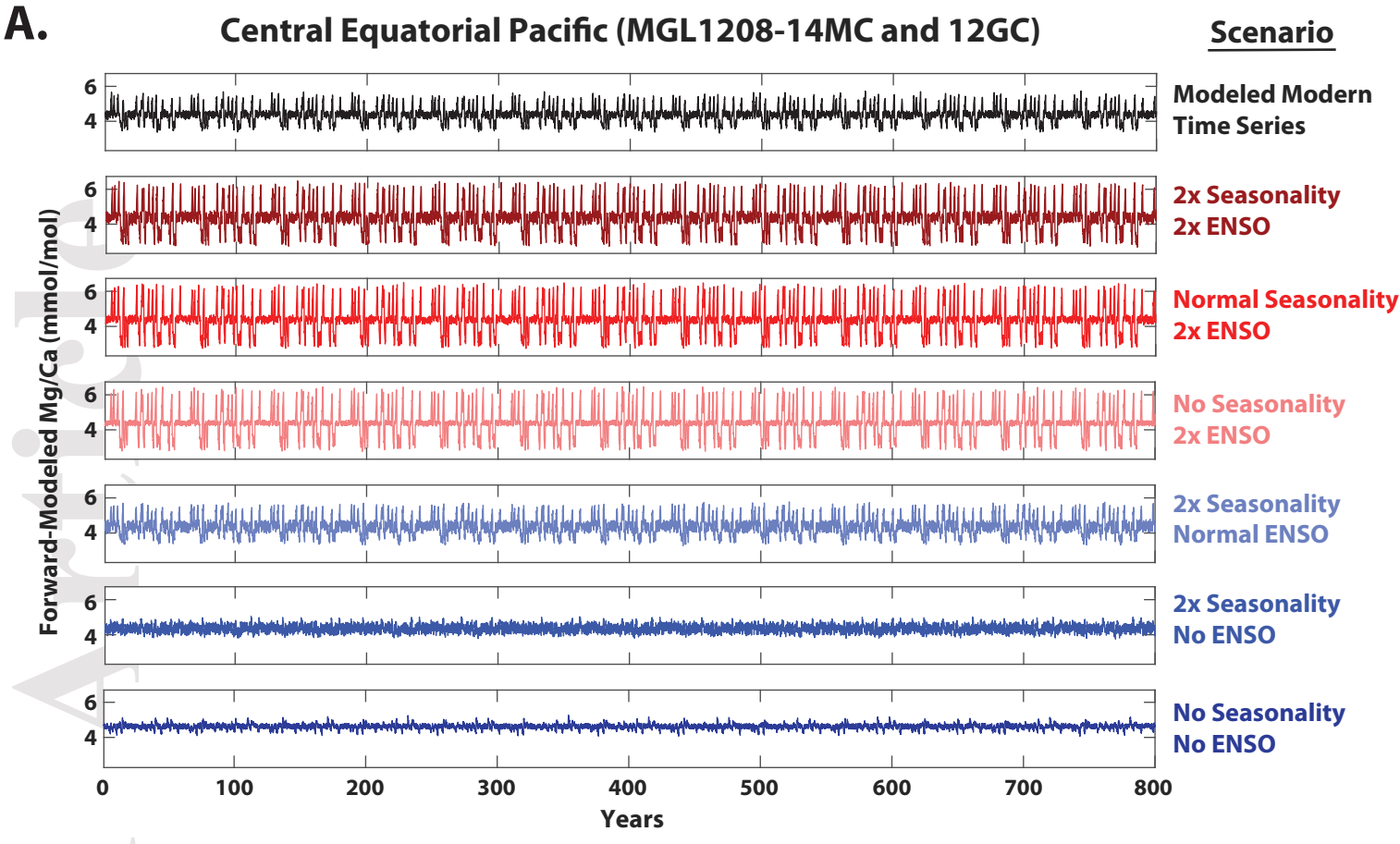


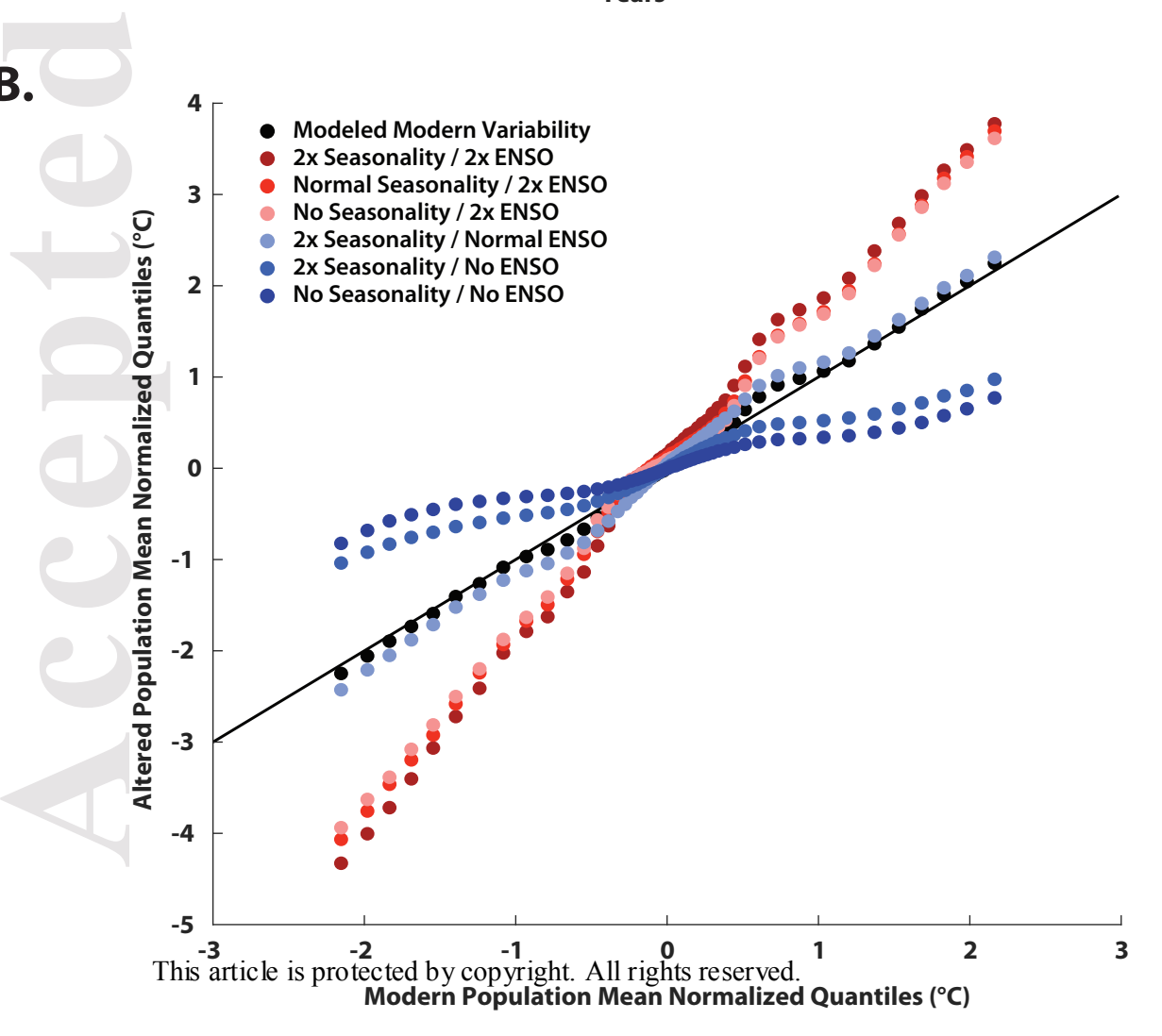


Western Tropical Pacific (MD06-3018)

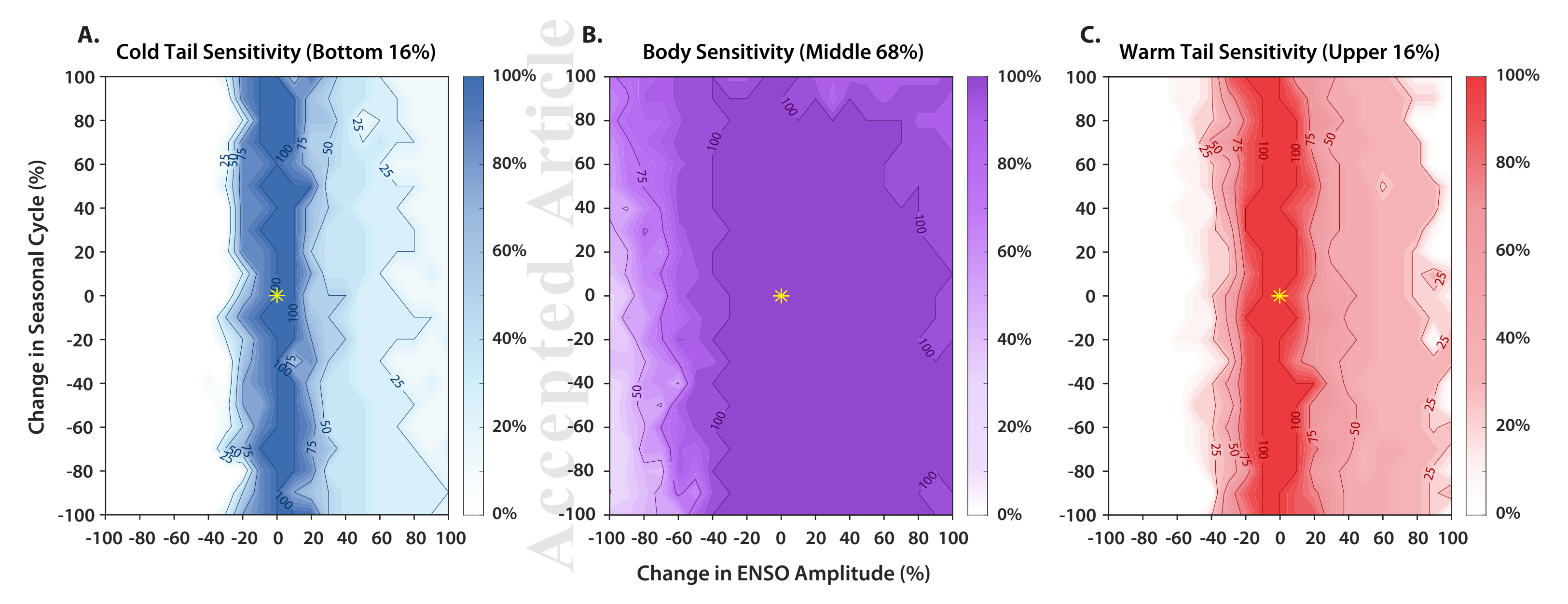




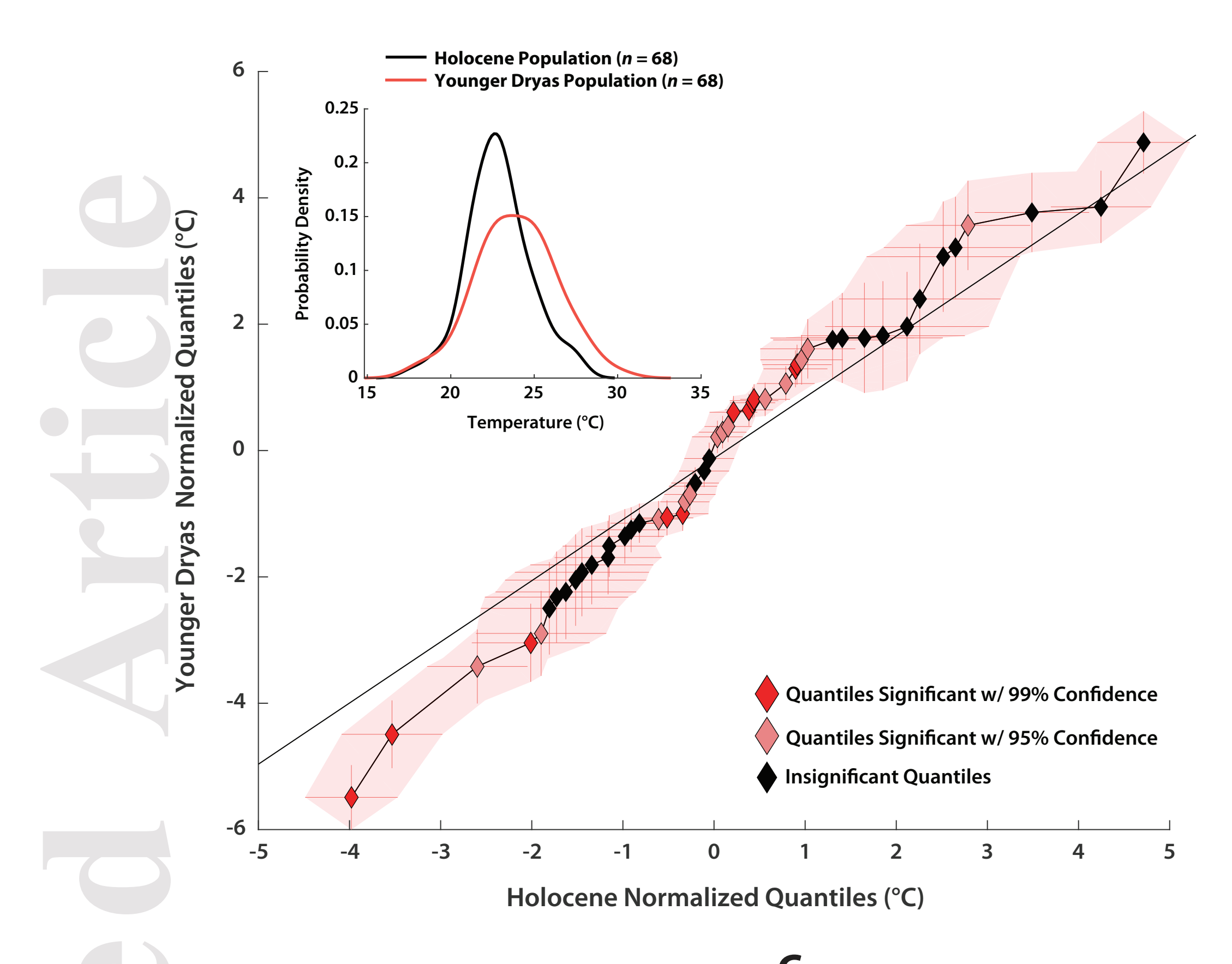


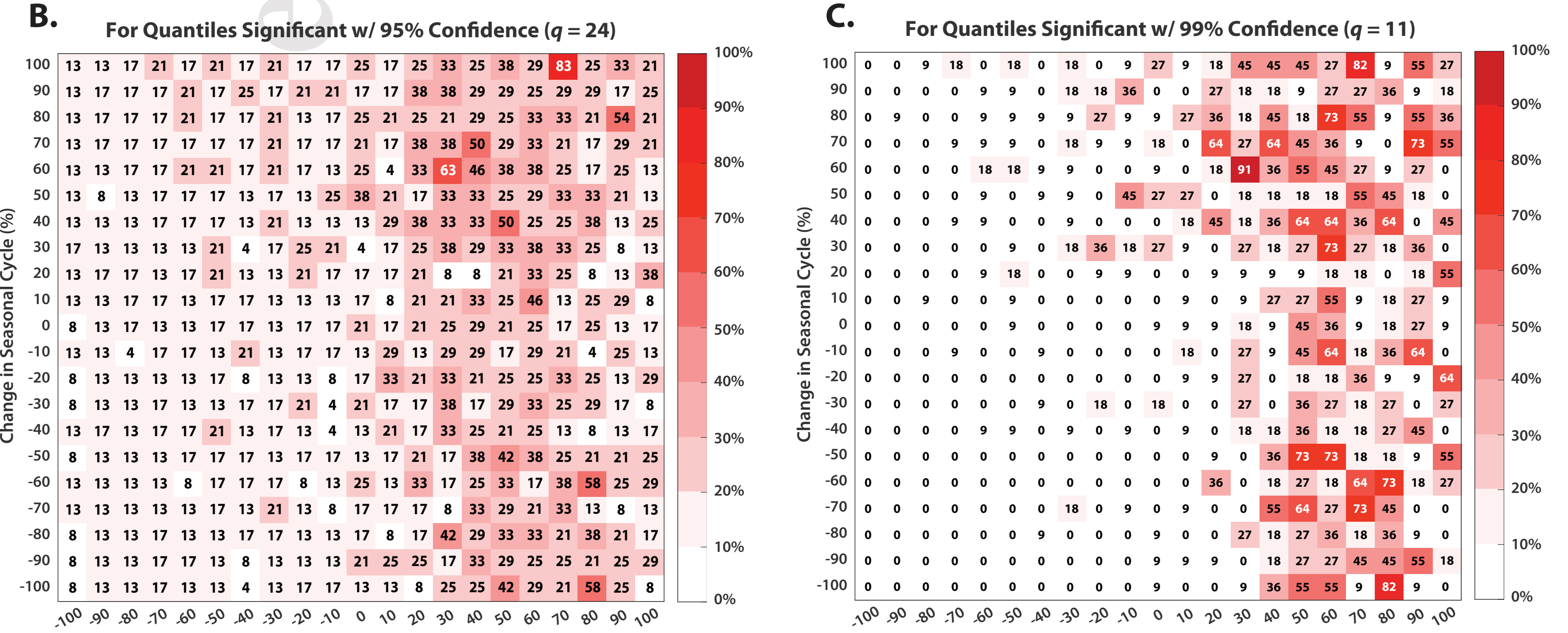


Central Equatorial Pacific (MGL1208-14MC and 12GC)



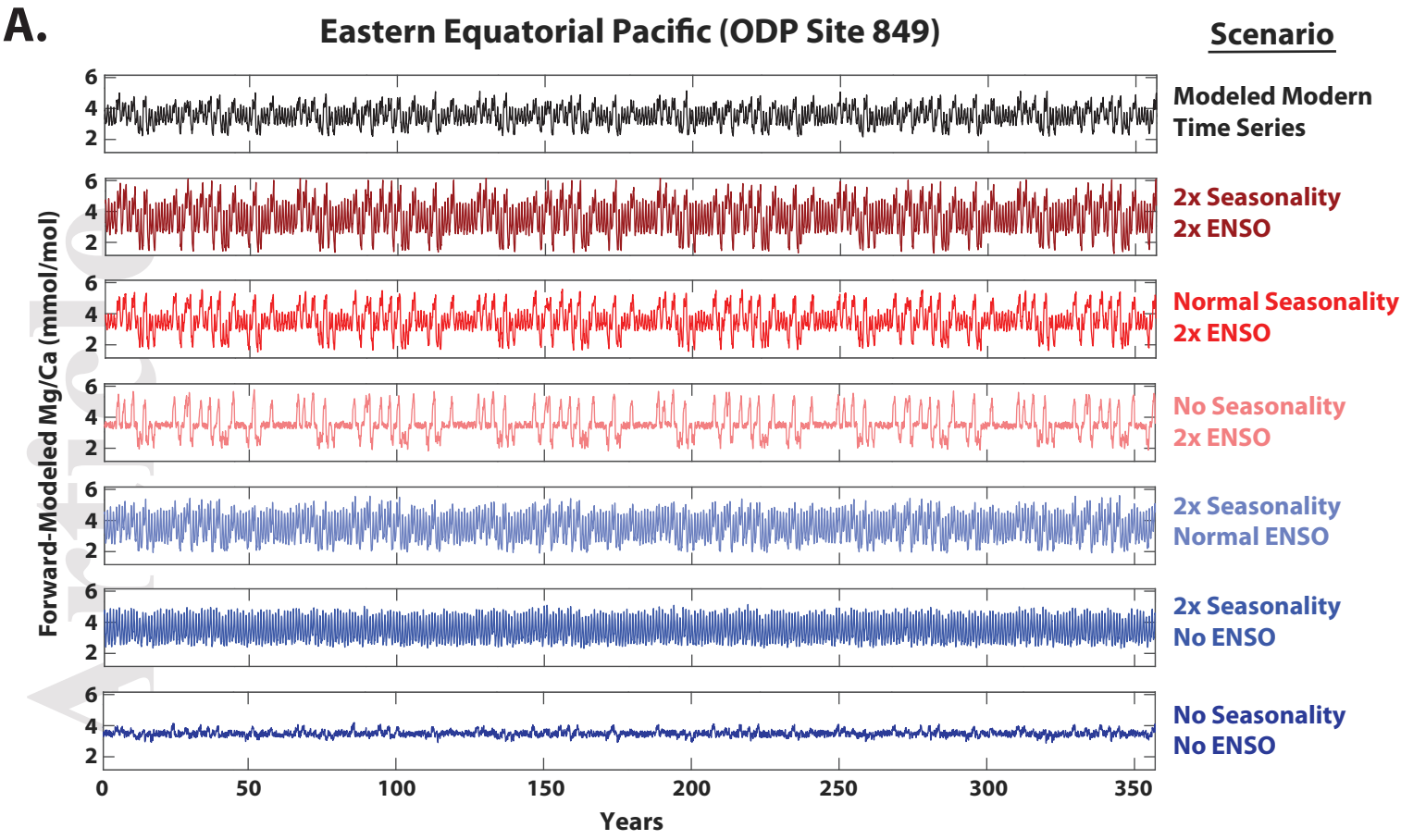


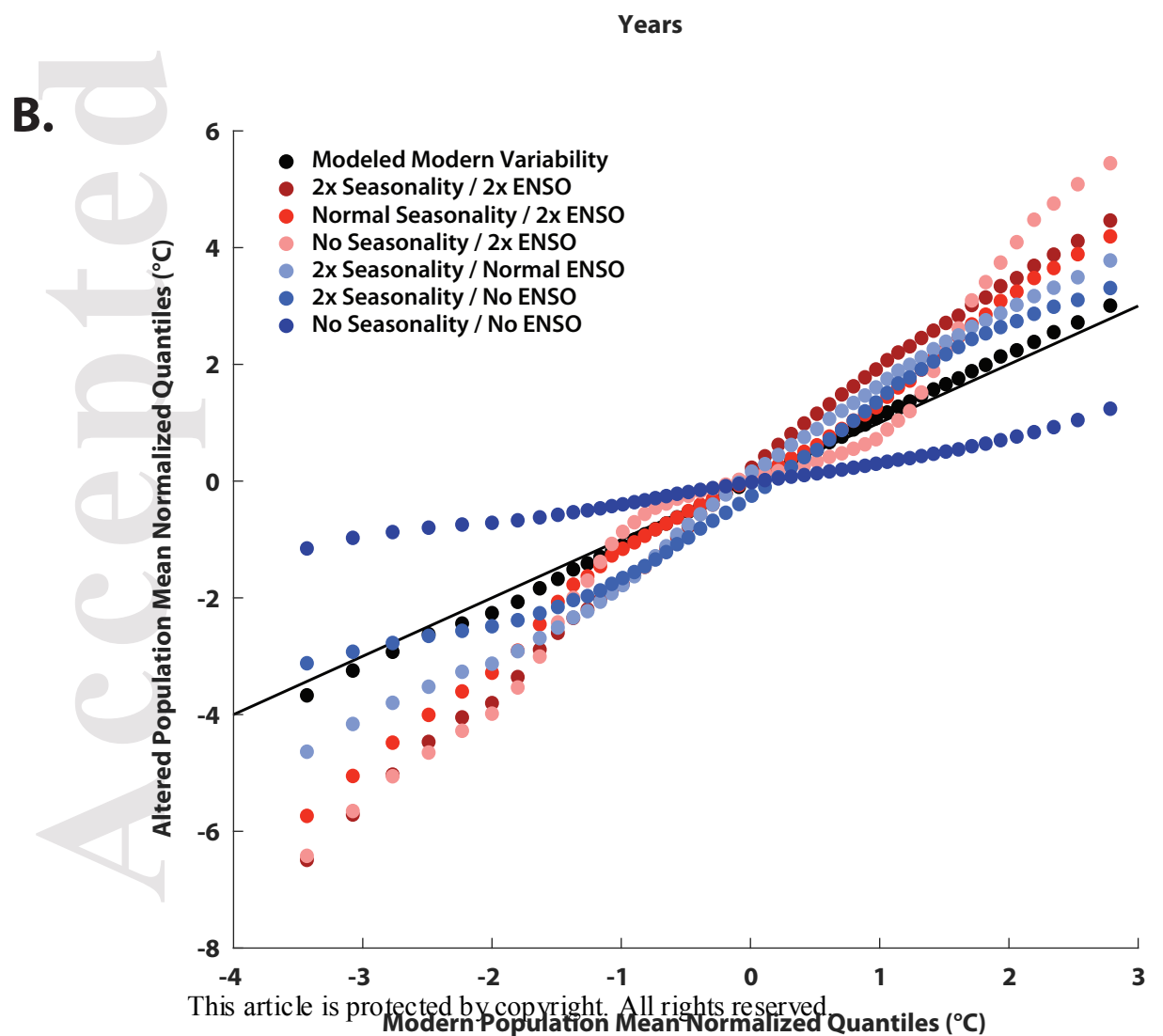




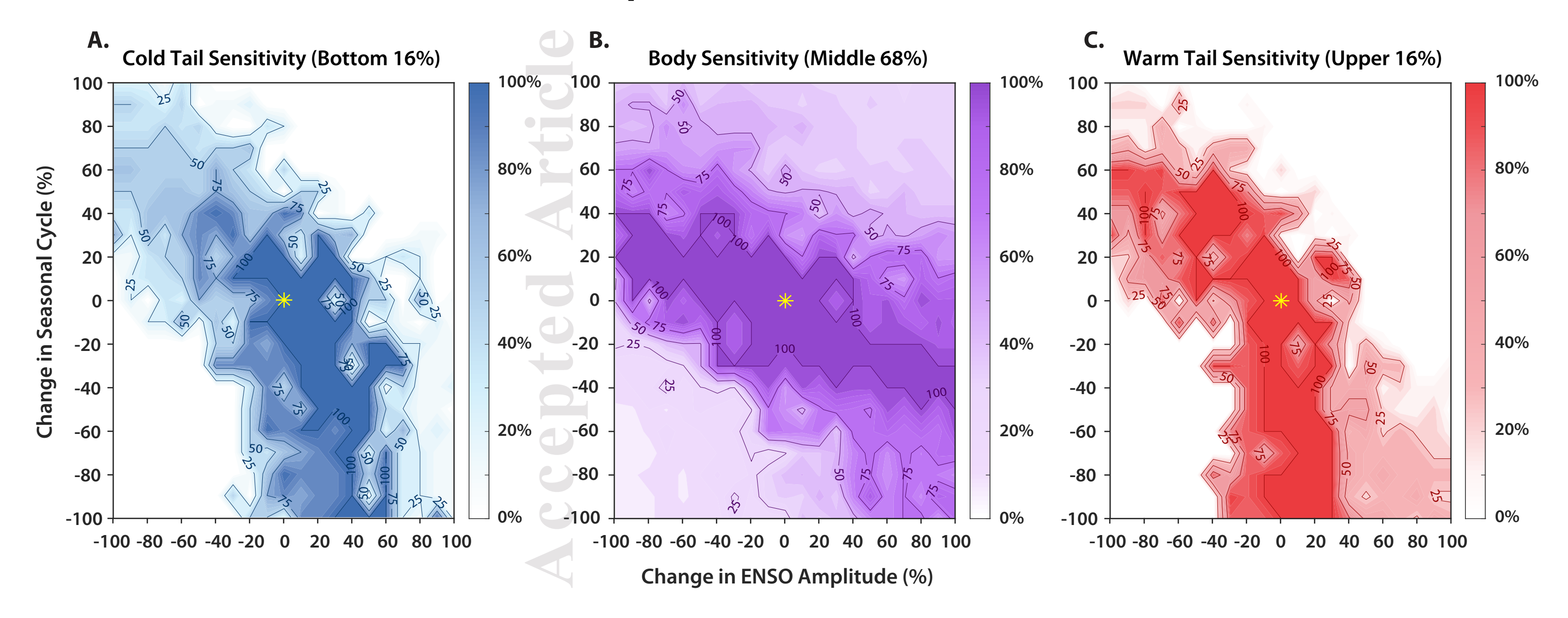
Change in ENSO Amplitude (%)

Change in ENSO Amplitude (%)
This article is protected by copyright. All rights reserved.

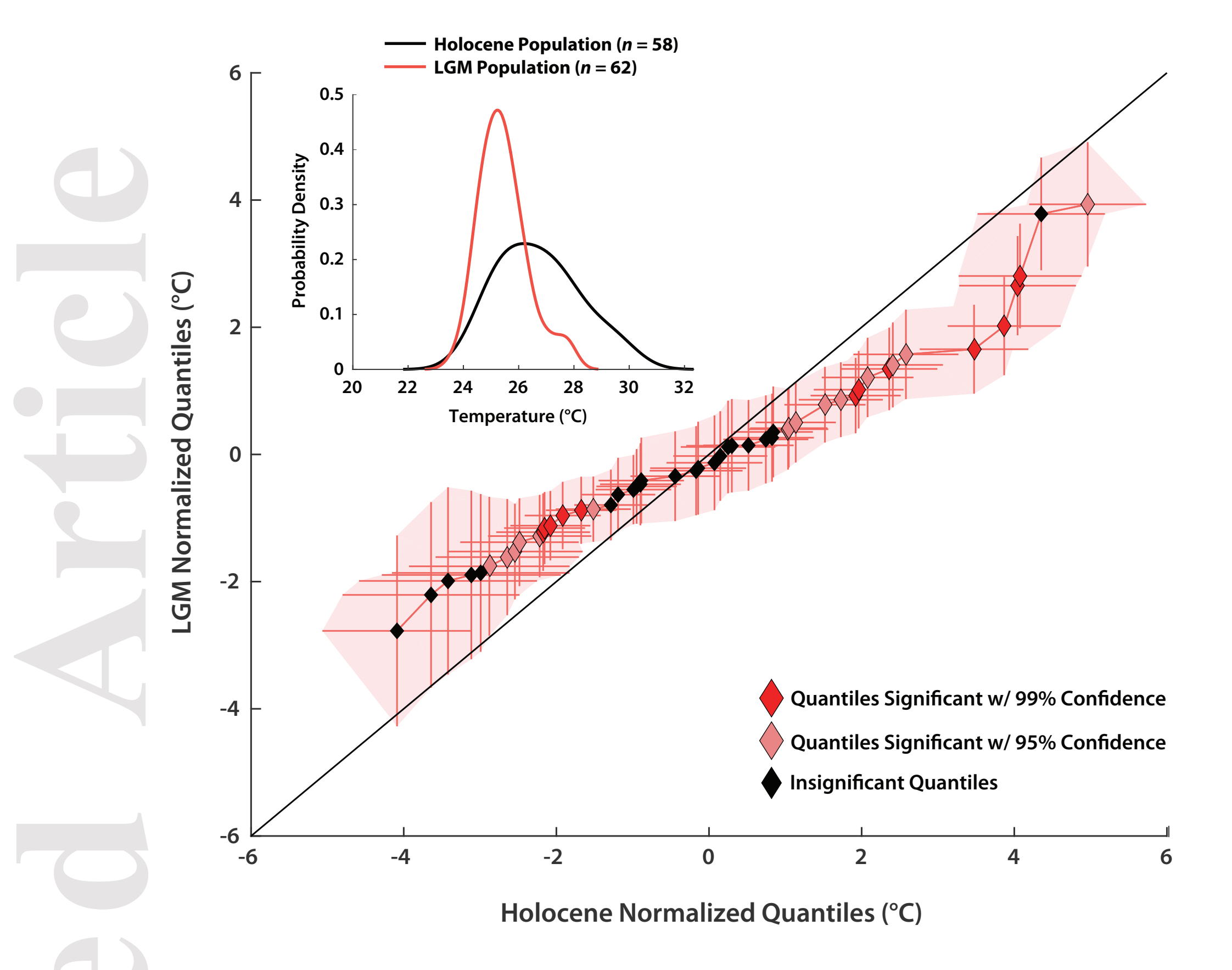


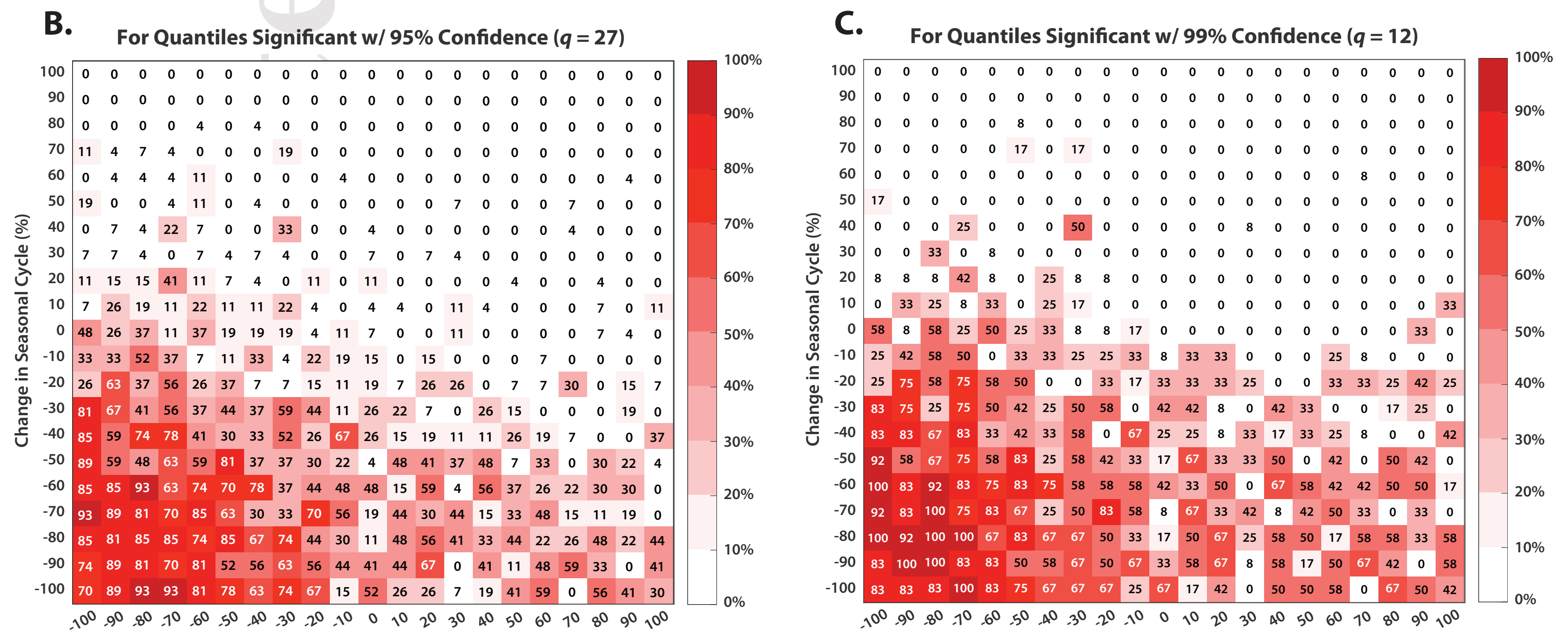


Eastern Equatorial Pacific (ODP Site 849)









Change in ENFO: Amplitudes protected by copyright. All rights reserved.

Change in ENSO Amplitude (%)

Parameter	Variable	Description
Individual Foraminiferal Data	a	
Reference Population	X	IFA Population to be plotted along the X-axis [Omit if performing sensitivity analysis]
Comparison Population	Y	IFA Population to be plotted along the Y-axis [Omit if performing sensitivity analysis]
Reanalysis Data		
ORA-S5 Data Structure		A subset of Ocean Reanalysis System 5 potential temperature data (available for download).
Core Location		
Latitude	lat	Latitude of the core location (XX.5°)
Longitude	lon	Longitude of the core location (XX°)
Depth	dep	Mean calcification depth for foraminiferal species of interest
Calibration Equation	_	
Calibration Equation	eqn	Select from a bank of preloaded Mg/Ca-T calibrations (see Table S1) or program your own.
Dissolution Correction	D	For preloaded calibration equations that incorporate dissolution correction terms, the term (in km core depth, [CO ₃ ²⁻], or any other variable) can be entered here.
Initializing Conditions		
Number of Picked "Foraminifera"	num_p	No. of individuals in pseudo-IFA populations "picked" by QUANTIFA.
Number of Quantiles	num_q	No. of quantiles computed from pseudo-IFA data (ideally $num_q < nump_p$).
Seasonal Weighting	seas	Months weighted in QUANTIFA's picking algorithm $(1 - 12 \text{ by default})$.
Pseudoproxy Time Series Length	tsl	Length (in yrs) of the pseudoproxy time series (equal to sampling resolution if running IFA data).
Model Realizations	run	No. of pseudo-IFA populations (and, by extension, Q-Q realizations) generated by QUANTIFA.
False Positive Rate Exercises	fp	No. of false positive rate exercises (recommended: $100 \text{ for } run = 1000 - 5000$)
Confidence Level	cl	Confidence level for uncertainty envelopes (85%, 90%, 95%, or 99%)
Analytical Error	anerr	Analytical uncertainty (in mmol/mol) from IFA measurements (choose a generic value, e.g. 0.1 mmol/mol, if running sensitivity tests).
Calibration Error	calerr	Error (in °C) for the selected calibration equation. [OPTIONAL]